Research Article

Daniele Boffi, Ramon Codina, and Önder Türk*

Finite element formulations for Maxwell's eigenvalue problem using continuous Lagrangian interpolations

https://doi.org/10.1515/sample-YYYY-XXXX
Received Month DD, YYYY; revised Month DD, YYYY; accepted Month DD, YYYY

Abstract: We consider nodal-based Lagrangian interpolations for the finite element approximation of the Maxwell eigenvalue problem. The first approach introduced is a standard Galerkin method on Powell-Sabin meshes, which has recently been shown to yield convergent approximations in two dimensions, whereas the other two are stabilized formulations that can be motivated by a variational multiscale approach. For the latter, a mixed formulation equivalent to the original problem is used, in which the operator has a saddle point structure. The Lagrange multiplier introduced to enforce the divergence constraint vanishes in an appropriate functional setting. The first stabilized method consists of an augmented formulation including a mesh dependent term that can be regarded as the Laplacian of the divergence constraint multiplier. The second formulation is based on orthogonal projections, which can be recast as a residual based stabilization technique. We rely on the classical spectral theory to analyze the approximating methods for the eigenproblem. The stability and convergence aspects are inherited from the associated source problems together with an assumption which is discussed numerically. We investigate the performance of the proposed formulations and provide some convergence results validating the theoretical ones for several benchmark tests, including ones with smooth and singular solutions.

Keywords: Maxwell eigenvalue problem, Stabilized finite elements, Lagrange elements

1 Introduction

The main object of this paper is to approximate the Maxwell eigenvalue problem (EVP) which, for instance, can be considered as the problem of determining resonances in a perfectly conducting cavity and the associated nontrivial time harmonic electric field (see, e.g., [7, 15, 25]). Defined on a bounded polyhedral domain Ω in $\mathbb{R}^d$, $d = 2, 3$, the EVP we consider consists of finding $[\boldsymbol{u}, \lambda]$, where $\lambda \in \mathbb{R}$, such that

$$\begin{cases} \mu \nabla \times \nabla \times \boldsymbol{u} = \lambda \boldsymbol{u} & \text{in } \Omega, \\ \nabla \cdot \boldsymbol{u} = 0 & \text{in } \Omega, \\ \boldsymbol{n} \times \boldsymbol{u} = \boldsymbol{0} & \text{on } \partial\Omega, \end{cases} \tag{1}$$

where μ is a positive parameter taken in accordance with the physical assumptions on the problem setting.

This EVP is of fundamental importance in computational electromagnetism. An active intense research is ongoing in the development of finite element (FE) methods that are capable of correctly approximating the constitutive and topological relations by this and other Maxwell systems. It is well known that the use of the curl conforming Nédélec or edge elements (rotated Raviart-Thomas elements in two dimensions) providing continuity of the tangential

Daniele Boffi, King Abdullah University of Science and Technology, Thuwal 23955-6900, Saudi Arabia, and University of Pavia, Pavia 27100, Italy
Ramon Codina, Universitat Politècnica de Catalunya, and International Centre for Numerical Methods in Engineering (CIMNE), 08034 Barcelona, Spain
***Corresponding author: Önder Türk,** Institute of Applied Mathematics, Middle East Technical University, 06800 Ankara, Turkey, e-mail: onder.turk@yandex.com

vector components while leaving the normal field components discontinuous across interfaces, results in convergent (spurious-free) approximations. The Nédélec elements provide a natural basis for the finite element methods that satisfy the discrete inf-sup condition [8, 24] and, furthermore, Dirichlet conditions on the tangent component of the vector unknown are easy to impose, which is not as clear using nodal elements; this issue is partially touched in this paper. However, as the continuity of the tangential field is inherent along the boundaries, a normal continuity may also be concerned and, moreover, there are situations such as time dependent problems and coupled problems where the edge elements do not provide optimal implementation and approximation properties. Thus, there are evident reasons to require the use of Lagrange finite elements with low order interpolations and less constraints on the problem domain discretization. In search for this, an equivalent problem to (1) can be obtained by reformulating it as a saddle point problem by the enforcement of the divergence constraint using a Lagrange multiplier p. In this case, the given system is governed by the Euler-Lagrange equations given as: find $[\boldsymbol{u}, p, \lambda]$, where $\lambda \in \mathbb{R}$, such that

$$\begin{cases} \mu \nabla \times \nabla \times \boldsymbol{u} + \nabla p = \lambda \boldsymbol{u} & \text{in } \Omega, \\ \nabla \cdot \boldsymbol{u} = 0 & \text{in } \Omega, \\ \boldsymbol{n} \times \boldsymbol{u} = \boldsymbol{0} \text{ and } p = 0 & \text{on } \partial\Omega. \end{cases} \tag{2}$$

The mixed variational form of this problem is also known as the Kikuchi formulation [8, 23].

On the other hand, it is well known that the use of standard nodal continuous Galerkin FE schemes to approximate the standard Maxwell systems has the pathology of producing spurious or non physical solutions even on smooth domains. There are many strategies consisting of penalization or regularizing the operator by adding a term containing the divergence. We refer for instance to [4, 5, 8, 11, 17], and the inclusive list of references therein on the subject. Also, mixed methods consisting of inf-sup stable elements using nodal continuous Lagrange elements of any order for the vector field together with a piecewise constant approximation for the multiplier have been proposed in recent works [20, 21].

In this paper, our main interest is to approximate the eigenvalues and eigenfunctions of the Maxwell operator without spurious solutions, using continuous Lagrange finite elements. Firstly we consider the standard Galerkin approximation on Powell-Sabin triangulations, where the convergence of the eigenvalues is provided in a recent work [11] (see also the three dimensional generalization in [10]). Next, the mixed FE formulations based on two stabilized forms are presented; a so called augmented formulation, and a formulation that is based on projections. The first stabilized method provides pressure stability by inclusion of a least squares form of the divergence constraint introduced for the corresponding source problem in [4]. The second approach is based on stabilizing the divergence and gradient components that are orthogonal to the associated FE spaces, which is analyzed in [3]. A reinterpretation of these two methods in a unified framework with a brief analysis of their key properties has also been given in [5].

The outline of the paper is as follows. In Section 2 we briefly describe the standard Galerkin method on Powell-Sabin meshes, whereas the two stabilized formulations are described in Section 3. While the EVP is directly analyzed for the Galerkin method, convergence results for the stabilized formulations rely on a suitable approximation of the source problem and the classical spectral theory, which is applied in Section 4. The main objective of this work is to check and compare the performance of nodal based formulations for the problem at hand, and this is done in Section 5. Finally, some conclusions are drawn in Section 6.

2 The standard Galerkin approximation with Powell-Sabin meshes

The variational formulation of (1) is given as follows: find $\boldsymbol{u} \in H_0(\mathbf{curl}, \Omega)$, $\boldsymbol{u} \neq \boldsymbol{0}$, and $\lambda \in \mathbb{R}$ satisfying

$$\mu(\nabla \times \boldsymbol{u}, \nabla \times \boldsymbol{v}) = \lambda(\boldsymbol{u}, \boldsymbol{v}), \quad \forall \boldsymbol{v} \in H_0(\mathbf{curl}, \Omega), \tag{3}$$

where $H(\mathbf{curl}, \Omega) = \{\boldsymbol{v} \in L^2(\Omega)^d : \nabla \times \boldsymbol{v} \in L^2(\Omega)^d\}$, $H_0(\mathbf{curl}, \Omega) = \{\boldsymbol{v} \in H(\mathbf{curl}, \Omega) : \boldsymbol{n} \times \boldsymbol{v} = \boldsymbol{0} \text{ on } \partial\Omega\}$, and $(\cdot, \cdot)$ denotes the L^2-inner product defined over Ω. Note that there is no need to enforce the divergence free condition for $\boldsymbol{u}$, as taking the divergence on both sides of the first equation in (1) directly yields that this field is divergence free.

For the FE approximation to this problem, let $\mathcal{T}_h$ be a partition of the problem domain Ω into a set of element domains $\{K\}$. As usual, h denotes the characteristic mesh size of the partition, here taken as $h = \max_{K\in\mathcal{T}_h} h_K$, where h_K is the diameter of the element K. Since our main interest is in the nodal approximations, we define the space of piecewise continuous polynomials on Ω as

$$\mathcal{N}_k(\Omega) = \{v_h \in \mathcal{C}^0(\bar{\Omega}) : v_h|_K \in \mathcal{P}_k(K), \quad \forall K \in \mathcal{T}_h\},$$

where $\mathcal{P}_k(K)$ denotes the space of polynomials of degree at most k defined on K. For the components of the vector fields as well as the scalar fields we will make use of these $H^1(\Omega)$-conforming approximating spaces in which every function can be determined uniquely by its values on the set of nodes of the defining elements. For all the analysis given in this work we assume for the sake of simplicity that the partitions are quasi-uniform. This assumption is compatible with the analysis given in [4], and can be relaxed by appropriate modifications in that work. We also make use of this quasi-uniformity assumption as a sufficient condition for the $H^1(\Omega)$-stability of the $L^2(\Omega)$-projection which can be procured under weaker assumptions (see, e.g., [6, 16]).

The Galerkin discretization on a finite dimensional space $\mathcal{V}_h$ of partition size h, can be written as: find nonzero $\boldsymbol{u}_h \in \mathcal{V}_h$, and $\lambda_h \in \mathbb{R}$ such that

$$\mu(\nabla \times \boldsymbol{u}_h, \nabla \times \boldsymbol{v}_h) = \lambda(\boldsymbol{u}_h, \boldsymbol{v}_h), \quad \forall \boldsymbol{v}_h \in \mathcal{V}_h. \tag{4}$$

As we have already mentioned, it is known that when $\mathcal{V}_h$ is taken as the $H^1(\Omega)$-conforming Lagrange FE space spurious solutions may exist for an arbitrary mesh size (see [8, 11], and the references therein). An example to such pathology will be given in Section 5. On the other hand, it has been proved in [11] that the standard formulation when implemented by the use of linear Lagrange finite elements on Powell-Sabin triangulations yields convergence of the eigenvalues to the true ones; the analysis presented in this reference is not based on the approximation properties of the method for the source problem, since it is not well posed. We will also include a numerical evidence for this in Section 5.

3 Stabilized formulations

The two stabilized formulations we shall consider are based on the Kikuchi formulation (2) of the EVP. There are essentially two alternatives for the variational form of this formulation, depending on whether the term with p is integrated by parts or not, as this inherently implies two possible choices for the functional framework of the problem [4, 5]. Consistently with the Galerkin approximation described earlier, we consider only the so called curl formulation, in which the pressure gradient is not integrated by parts and the space where the solution is sought is $\mathcal{X} = H_0(\mathbf{curl}, \Omega) \times H_0^1(\Omega)$. The problem then reads: find $[\boldsymbol{u}, p] \in \mathcal{X}$ and $\lambda \in \mathbb{R}$ such that

$$B([\boldsymbol{u}, p], [\boldsymbol{v}, q]) = \lambda(\boldsymbol{u}, \boldsymbol{v}), \quad \forall [\boldsymbol{v}, q] \in \mathcal{X}, \tag{5}$$

where

$$B([\boldsymbol{u}, p], [\boldsymbol{v}, q]) = \mu(\nabla \times \boldsymbol{u}, \nabla \times \boldsymbol{v}) + (\nabla p, \boldsymbol{v}) - (\nabla q, \boldsymbol{u}).$$

Let $\mathcal{V}_h \subset \mathcal{V} := H_0(\mathbf{curl}, \Omega)$ and $\mathcal{Q}_h \subset \mathcal{Q} := H_0^1(\Omega)$ be the FE spaces to approximate $\boldsymbol{u}$ and p, respectively. The Galerkin approximation of the variational problem in $\mathcal{X}_h = \mathcal{V}_h \times \mathcal{Q}_h \subset \mathcal{X}$ is given as: find $[\boldsymbol{u}_h, p_h] \in \mathcal{X}_h$ and $\lambda_h \in \mathbb{R}$ such that

$$B([\boldsymbol{u}_h, p_h], [\boldsymbol{v}_h, q_h]) = \lambda_h(\boldsymbol{u}_h, \boldsymbol{v}_h), \quad \forall [\boldsymbol{v}_h, q_h] \in \mathcal{X}_h. \tag{6}$$

The corresponding source problem is well posed in spaces $\mathcal{V}_h$ and $\mathcal{Q}_h$ if they satisfy the discrete inf-sup condition

$$\inf_{p_h\in\mathcal{Q}_h} \sup_{\boldsymbol{v}_h\in\mathcal{V}_h} \frac{(\nabla p_h, \boldsymbol{v}_h)}{\|p_h\|_{\mathcal{Q}}\|\boldsymbol{v}_h\|_{\mathcal{V}}} \geq K_b, \tag{7}$$

($\|\cdot\|_{\mathcal{B}}$ standing for the norm in a space $\mathcal{B}$) for a certain constant $K_b > 0$, and this is a sufficient condition for the EVP to be well-posed. Examples of pairs of spaces satisfying this condition are those based on Nédélec's elements to construct $\mathcal{V}_h$ and nodal Lagrangian continuous elements to construct $\mathcal{Q}_h$. However, as it has been mentioned, we are interested in arbitrary nodal-based interpolations, in which case the spaces $\mathcal{V}_h$ and $\mathcal{Q}_h$ may fail to fulfill condition (7). As explained in the previous section, there is also the possibility to use the Galerkin method with nodal elements without introducing the Lagrange multiplier p if the FE mesh is of Powell-Sabin type.

The alternative is to switch to a stabilized FE approximation to approximate the eigenproblem given in (5). In order to prove that the solutions of the stabilized formulations converge to the solutions of the continuous problem, we will apply the classical spectral approximation theory relying on the convergence of the associated source problem for arbitrary forcing terms, not necessarily solenoidal. This is what we analyze next.

3.1 Source problem with non-solenoidal forcing terms

The continuous source problem associated to the Maxwell EVP reads as follows: given a vector field $\boldsymbol{f} \in L^2(\Omega)^d$, not necessarily solenoidal, find $[\boldsymbol{u}, p] \in \mathcal{X}$ such that

$$B([\boldsymbol{u}, p], [\boldsymbol{v}, q]) = (\boldsymbol{f}, \boldsymbol{v}), \quad \forall [\boldsymbol{v}, q] \in \mathcal{X}. \tag{8}$$

Since now $\nabla \cdot \boldsymbol{f} \neq 0$ in general, $p \neq 0$. We may consider the Helmholtz decomposition $\boldsymbol{f} = \boldsymbol{f}_0 + \nabla\phi$, where ϕ is the solution of the problem

$$\begin{aligned} -\Delta\phi &= -\nabla\cdot\boldsymbol{f} && \text{in } \Omega, \\ \phi &= 0 && \text{on } \partial\Omega, \end{aligned}$$

so that $\boldsymbol{f}_0 = \boldsymbol{f} - \nabla\phi$ is such that $\nabla \cdot \boldsymbol{f}_0 = 0$ and $\boldsymbol{n} \times \boldsymbol{f}_0 = \boldsymbol{n} \times \boldsymbol{f}$ on $\partial\Omega$. It is immediately checked that the solution of the problem

$$\begin{cases} \mu\nabla\times\nabla\times\boldsymbol{u} + \nabla p = \boldsymbol{f}_0 + \nabla\phi & \text{in } \Omega, \\ \nabla\cdot\boldsymbol{u} = 0 & \text{in } \Omega, \\ \boldsymbol{n}\times\boldsymbol{u} = \boldsymbol{0} \text{ and } p = 0 & \text{on } \partial\Omega. \end{cases} \tag{9}$$

is $p = \phi$ and $\boldsymbol{u}$ the solution of the source problem with solenoidal forcing term $\boldsymbol{f}_0$. We need to slightly modify the formulations proposed in [4] and [3] for the source problem with solenoidal forcing terms to take this fact into account. The formulations we actually propose can be written as follows: find $[\boldsymbol{u}_h, p_h] \in \mathcal{X}_h$ such that

$$B_{\mathrm{S}}([\boldsymbol{u}_h, p_h], [\boldsymbol{v}_h, q_h]) = L_{\mathrm{S}}([\boldsymbol{v}_h, q_h]), \quad \forall [\boldsymbol{v}_h, q_h] \in \mathcal{X}_h, \tag{10}$$

where $B_{\mathrm{S}}([\boldsymbol{u}_h, p_h], [\boldsymbol{v}_h, q_h])$ and $L_{\mathrm{S}}([\boldsymbol{v}_h, q_h])$ are defined as

$$\begin{aligned} B_{\mathrm{S}}([\boldsymbol{u}_h, p_h], [\boldsymbol{v}_h, q_h]) &= B([\boldsymbol{u}_h, p_h], [\boldsymbol{v}_h, q_h]) \\ &\quad + \sum_K \tau_p(\tilde{P}(\nabla p_h), \tilde{P}(\nabla q_h))_K \\ &\quad + \sum_K \tau_{\boldsymbol{u}}(\tilde{P}(\nabla\cdot\boldsymbol{u}_h), \tilde{P}(\nabla\cdot\boldsymbol{v}_h))_K, \end{aligned} \tag{11}$$

$$L_{\mathrm{S}}([\boldsymbol{v}_h, q_h]) = (\boldsymbol{f}, \boldsymbol{v}_h) + \sum_K \tau_p(\tilde{P}(\nabla\phi), \tilde{P}(\nabla q_h))_K. \tag{12}$$

The difference with respect to the formulations proposed in [4] and [3] is the second term in $L_{\mathrm{S}}([\boldsymbol{v}_h, q_h])$. In the above equation $\sum_K$ signifies the summation over all elements K of the partition, and $(\cdot,\cdot)_K$ denotes the $L^2(K)$-inner product. The stabilization parameters are defined as follows

$$\tau_p = c_p \frac{\ell^2}{\mu}, \quad \tau_{\boldsymbol{u}} = c_{\boldsymbol{u}}\mu\frac{h^2}{\ell^2},$$

where c_p and $c_{\boldsymbol{u}}$ are appropriately chosen algorithmic constants and ℓ is a length scale of the problem. It is observed that these parameters are constant in the case of quasi-uniform FE partitions (i.e., using the same h for all elements) and constant μ. Otherwise, they should be computed element-wise; this is why we have introduced the summation over the elements, which is in fact not needed in our case.

The method depends on the projection $\tilde{P}$ which can be either the identity I or the orthogonal projection to the FE space, $P_h^{\perp}$, leading to the augmented (AG) and the orthogonal subgrid scale (OSGS) formulations, respectively. This orthogonal projection can be computed as $P_h^{\perp} = I - P_h$, P_h being the $L^2(\Omega)$-projection onto the FE space, either $\mathcal{V}_h$ or $\mathcal{Q}_h$; we have not distinguished these two possibilities, being clear by the context the projection to consider. The bilinear form B_{S} in (10) will be denoted by B_{AG} when $\tilde{P} = I$, and by B_{OSGS} when $\tilde{P} = P_h^{\perp}$. The OSGS formulation is a residual-based stabilized discretization where only the components of the divergence and gradient terms in (11) that are orthogonal to the corresponding FE spaces are stabilized [3, 5]. The orthogonal projections onto the corresponding space can be computed iteratively or treated implicitly. We will follow the latter option in the numerical results presented for this study.

The stability and convergence of the AG and OSGS formulations for the source problems are analyzed in [4] and [3], respectively, when $\nabla \cdot \boldsymbol{f} = 0$. The reason for the modification introduced in this paper is to have consistency even when $\nabla \cdot \boldsymbol{f} \neq 0$. It is trivially verified that if $[\boldsymbol{u}, p]$ is the solution of the continuous problem, for which we know that $p = \phi$, there holds

$$B_{\mathrm{S}}([\boldsymbol{u}, p], [\boldsymbol{v}_h, q_h]) = L_{\mathrm{S}}([\boldsymbol{v}_h, q_h]) \quad \forall [\boldsymbol{v}_h, q_h] \in \mathcal{X}_h,$$

from where we have the consistency property

$$B_{\mathrm{S}}([\boldsymbol{u} - \boldsymbol{u}_h, p - p_h], [\boldsymbol{v}_h, q_h]) = 0 \quad \forall [\boldsymbol{v}_h, q_h] \in \mathcal{X}_h. \tag{13}$$

Despite both the AG and the OSGS methods yielding good results, the norm in which stability and convergence can be proved is weaker for the latter than for the former. Let us start with the AG formulation. The norm in which the numerical analysis of the source problem can be done is

$$\|[\boldsymbol{v}, q]\|_{\mathrm{AG}}^2 := \mu \|\nabla \times \boldsymbol{v}\|_{L^2(\Omega)}^2 + \frac{\mu}{\ell^2} \|\boldsymbol{v}\|_{L^2(\Omega)}^2 + \frac{\ell^2}{\mu} \|\nabla q\|_{L^2(\Omega)}^2 + \mu \frac{h^2}{\ell^2} \|\nabla \cdot \boldsymbol{v}\|_{L^2(\Omega)}^2, \tag{14}$$

which is a norm in $\mathcal{X}$ with adequate scaling coefficients and additional (but weak) control on the divergence of $\boldsymbol{v}$.

In the sequel, $\lesssim$ denotes an inequality up to a positive constant that is independent of the mesh size and the problem coefficients.

We have the following result:

Theorem 1. *Suppose that both $\mathcal{V}_h$ and $\mathcal{Q}_h$ are constructed using continuous nodal based interpolations, each of arbitrary degree. Then, problem (10) (with $B_{\mathrm{S}} = B_{\mathrm{AG}}$) is well posed, in the sense that it admits a unique solution $[\boldsymbol{u}_h, p_h] \in \mathcal{V}_h \times \mathcal{Q}_h$ that satisfies*

$$\|[\boldsymbol{u}_h, p_h]\|_{\mathrm{AG}} \lesssim \frac{\ell}{\mu^{1/2}} \|\boldsymbol{f}\|_{L^2(\Omega)}. \tag{15}$$

Furthermore, $[\boldsymbol{u}_h, p_h]$ converges optimally as $h \to 0$ to the solution $[\boldsymbol{u}, p] \in \mathcal{V} \times \mathcal{Q}$ of the continuous problem (8), in the following sense:

$$\|[\boldsymbol{u} - \boldsymbol{u}_h, p - p_h]\|_{\mathrm{AG}} \lesssim \inf_{[\boldsymbol{v}_h, q_h] \in \mathcal{V}_h \times \mathcal{Q}_h} \|[\boldsymbol{u} - \boldsymbol{v}_h, p - q_h]\|_{\mathrm{AG}}. \tag{16}$$

Proof. The key property to obtain stability is the inf-sup condition for B_{AG} proved in [9]: given $[\boldsymbol{u}_h, p_h] \in \mathcal{V}_h \times \mathcal{Q}_h$, there exists $[\boldsymbol{v}_h, q_h] \in \mathcal{V}_h \times \mathcal{Q}_h$ such that

$$\|[\boldsymbol{u}_h, p_h]\|_{\mathrm{AG}} \|[\boldsymbol{v}_h, q_h]\|_{\mathrm{AG}} \lesssim B_{\mathrm{AG}}([\boldsymbol{u}_h, p_h], [\boldsymbol{v}_h, q_h]).$$

This implies that problem (10) has a unique solution, which will satisfy

$$\begin{aligned} \|[\boldsymbol{u}_h, p_h]\|_{\mathrm{AG}} \|[\boldsymbol{v}_h, q_h]\|_{\mathrm{AG}} &\lesssim L_{\mathrm{AG}}([\boldsymbol{v}_h, q_h]) \lesssim \|\boldsymbol{f}\|_{L^2(\Omega)} \|\boldsymbol{v}_h\|_{L^2(\Omega)} + \frac{\ell^2}{\mu} \|\nabla \phi\|_{L^2(\Omega)} \|\nabla q_h\|_{L^2(\Omega)} \\ &\lesssim \frac{\ell}{\mu^{1/2}} \left(\|\boldsymbol{f}\|_{L^2(\Omega)} + \|\nabla \phi\|_{L^2(\Omega)} \right) \left(\frac{\mu^{1/2}}{\ell} \|\boldsymbol{v}_h\|_{L^2(\Omega)} + \frac{\ell}{\mu^{1/2}} \|\nabla q_h\|_{L^2(\Omega)} \right), \end{aligned}$$

from where the stability result (15) follows noting that $\|\boldsymbol{f}\|^2_{L^2(\Omega)} = \|\boldsymbol{f}_0\|^2_{L^2(\Omega)} + \|\nabla\phi\|^2_{L^2(\Omega)}$.

It is straightforward to check that

$$B_{\mathrm{AG}}([\boldsymbol{u}_h, p_h], [\boldsymbol{v}_h, q_h]) \lesssim \|[\boldsymbol{u}_h, p_h]\|_{\mathrm{AG}} \|[\boldsymbol{v}_h, q_h]\|_{\mathrm{AG}},$$

i.e., B_{AG} is continuous in the norm $\|\cdot\|_{\mathrm{AG}}$. This, together with the inf-sup condition cited and the consistency condition (13) allow one to prove the convergence estimate (16) in the usual manner. Details are omitted. □

The error estimate (16) is optimal for smooth solutions, that is, when $\boldsymbol{u}$ belongs to $H^r(\Omega)^d$ for $r \geq 1$. In this case we have

$$\|[\boldsymbol{u} - \boldsymbol{u}_h, p - p_h]\|_{\mathrm{AG}} \lesssim h^{t-1} \|\boldsymbol{u}\|_{H^t(\Omega)}, \tag{17}$$

where $t = \min\{r, k+1\}$, k being the order of the FE interpolation.

We can also consider lower regularity cases. For instance, it is known that $\boldsymbol{u} \in H^r(\Omega)^d$ for $r \geq 1/2$ when the domain is a Lipschitz polyhedron [1]. In the cases of solutions with Sobolev regularity $1/2 < r < 1$, the analysis in [4] shows that the convergence is also optimal if the FE meshes are able to interpolate optimally scalar functions of Sobolev regularity $r+1$, whose gradients are components of $\boldsymbol{u}$. This happens for example if the FE meshes are of Powell-Sabin type (see [4] and references therein for further discussion). More precisely, if $\mathcal{V}_h$ contains gradients of scalar functions that are vector fields in $\mathcal{N}_k(\Omega)^d \cap H_0(\mathrm{curl}, \Omega)$, then (see [4], Corollary 3.12):

$$\|[\boldsymbol{u} - \boldsymbol{u}_h, p - p_h]\|_{\mathrm{AG}} = O(h^{t-\epsilon}),$$

for any $\epsilon \in]0, t - 1/2[$ for $t = \min\{r, k\}$.

For the EVP analysis we will need to relate the $L^2(\Omega)$-norm of the error $\boldsymbol{u} - \boldsymbol{u}_h$ to the $L^2(\Omega)$-norm of the forcing term $\boldsymbol{f}$. This follows easily from Theorem 1 when $\boldsymbol{f}$ is divergence free assuming enough regularity in the domain Ω (see, e.g., [13, 18]). However, the situation is more delicate when $\boldsymbol{f}$ is not solenoidal, for instance in the case when $\boldsymbol{f} = \nabla\phi$. For $\boldsymbol{f}$ divergence free, it is not difficult to prove using standard duality arguments, and the corresponding regularity assumptions, that

$$\mu^{1/2} \|\boldsymbol{u} - \boldsymbol{u}_h\|_{L^2(\Omega)} \lesssim h \|[\boldsymbol{u} - \boldsymbol{u}_h, p - p_h]\|_{\mathrm{AG}} \quad (\text{with } p = 0 \text{ if } \nabla \cdot \boldsymbol{f} = 0). \tag{18}$$

A similar result for a general $\boldsymbol{f}$ is not so obvious. In [22] this is obtained for a stabilized first order form of Maxwell's problem using two main steps that rely on an assumption on the FE mesh (Assumption 4.1 in [22]), similar to that is used in [11]. The first step is a Poincaré-Steklov inequality (Lemma 4.3 in [22]), which can be directly used in our case, and the second is a duality argument (Lemmata 5.4 and 5.5 in [22]). Here we combine the assumptions used in these two steps into a single one, and state the following:

Assumption 1. *The FE mesh and the domain Ω are such that there holds:*

$$\mu^{1/2} \|\boldsymbol{u} - \boldsymbol{u}_h\|_{L^2(\Omega)} \lesssim h^s \ell^{1-s} \|[\boldsymbol{u} - \boldsymbol{u}_h, p - p_h]\|_{\mathrm{AG}}, \tag{19}$$

for some $s > 0$.

Note that, according to (18), $s = 1$ for divergence free $\boldsymbol{f}$. Weakening this assumption into smaller pieces as done in [22] is an objective that we leave for future work. In any case, and just for illustrative purposes, in Section 5 we present a numerical test for which we show that (19) holds (with $s = 1$) for a limiting forcing term $\boldsymbol{f} = \nabla\phi$ and ϕ strictly in $H^1_0(\Omega)$.

From Assumption 1 and Theorem 1 it immediately follows:

Corollary 1. *Under the conditions of Theorem 1 and accepting Assumption 1, there holds*

$$\frac{\mu^{1/2}}{\ell} \|\boldsymbol{u} - \boldsymbol{u}_h\|_{L^2(\Omega)} \lesssim \frac{\ell}{\mu^{1/2}} \left(\frac{h}{\ell}\right)^s \|\boldsymbol{f}\|_{L^2(\Omega)}. \tag{20}$$

Proof. From the stability of the continuous solution and from (15) it follows that

$$\|[\boldsymbol{u} - \boldsymbol{u}_h, p - p_h]\|_{\mathrm{AG}} \lesssim \frac{\ell}{\mu^{1/2}} \|\boldsymbol{f}\|_{L^2(\Omega)}.$$

The result follows using Assumption 1. □

Considering the decomposition $\boldsymbol{f} = \boldsymbol{f}_0 + \nabla\phi$ with $\nabla \cdot \boldsymbol{f}_0 = 0$, it can be shown that this result holds without Assumption 1 when $\boldsymbol{f} = \boldsymbol{f}_0$. The need to use Assumption 1 arises when ϕ is not vanishing and it cannot be assumed smoother than $H^1(\Omega)$.

Let us remark that, since $\nabla \cdot \boldsymbol{f}_0 = 0$ and the test functions $q_h \in \mathcal{Q}_h$ vanish on $\partial\Omega$, we have that

$$L_{\mathrm{AG}}([\boldsymbol{v}_h, q_h]) = (\boldsymbol{f}, \boldsymbol{v}_h) + \sum_K \tau_p(\nabla\phi, \nabla q_h)_K = (\boldsymbol{f}, \boldsymbol{v}_h) + \sum_K \tau_p(\boldsymbol{f}, \nabla q_h)_K.$$

This means that we do not actually need to compute the Helmholtz decomposition of $\boldsymbol{f}$, which would be only feasible numerically and of course would imply an additional cost.

Let us move now to the OSGS formulation, and introduce in this case the mesh dependent norm:

$$\|[\boldsymbol{v}, q]\|^2_{\mathrm{OSGS}} := \mu\|\nabla \times \boldsymbol{v}\|^2_{L^2(\Omega)} + \frac{\mu}{\ell^2}\|\boldsymbol{v}\|^2_{L^2(\Omega)} + \frac{\ell^2}{\mu}\|P_h^{\perp}(\nabla q)\|^2_{L^2(\Omega)} + \frac{h^2}{\mu}\|P_h(\nabla q)\|^2_{L^2(\Omega)}. \tag{21}$$

This norm is weaker than (14) because the component of the pressure gradient in $\mathcal{V}_h$ is multiplied by h^2 instead of ℓ^2, apart from the fact that we have not included the control on $\nabla \cdot \boldsymbol{v}$. Nevertheless, the numerical results obtained in [3] showed that the OSGS formulation is as stable as the AG one; we shall corroborate this fact in this paper in the context of Maxwell's EVP. Stability and convergence is proved in [3]; because of the proof-technique employed, the statements of these results slightly differ from those in Theorem 1, but the essence is the same, namely, stability and optimal convergence:

Theorem 2. *Suppose that both $\mathcal{V}_h$ and $\mathcal{Q}_h$ are constructed using continuous nodal based interpolations of arbitrary degree each. Then, problem (10) (with $B_{\mathrm{S}} = B_{\mathrm{OSGS}}$) is well posed, in the sense that*

$$\inf_{[\boldsymbol{u}_h, p_h] \in \mathcal{V}_h \times \mathcal{Q}_h} \sup_{[\boldsymbol{v}_h, q_h] \in \mathcal{V}_h \times \mathcal{Q}_h} \frac{B_{\mathrm{OSGS}}([\boldsymbol{u}_h, p_h], [\boldsymbol{v}_h, q_h])}{\|[\boldsymbol{u}_h, p_h]\|_{\mathrm{OSGS}} \|[\boldsymbol{v}_h, q_h]\|_{\mathrm{OSGS}}} \geq K_{B_{\mathrm{OSGS}}} > 0. \tag{22}$$

Furthermore, $[\boldsymbol{u}_h, p_h]$ converges optimally as $h \to 0$ to the solution $[\boldsymbol{u}, p] \in V \times Q$ of the continuous problem (8), in the following sense:

$$\|[\boldsymbol{u} - \boldsymbol{u}_h, p - p_h]\|_{\mathrm{OSGS}} \lesssim \inf_{q_h \in \mathcal{Q}_h} \|[\boldsymbol{u} - P_{\mathcal{V}_h}(\boldsymbol{u}), p - q_h]\|_{\mathrm{OSGS}} + \inf_{\boldsymbol{v}_h \in \mathcal{V}_h} \mu^{1/2}\|\nabla \times \boldsymbol{u} - \boldsymbol{v}_h\|, \tag{23}$$

where $P_{\mathcal{V}_h}$ is the $L^2(\Omega)$-projection onto $\mathcal{V}_h$.

This result corresponds to Theorems 3.3 and 3.4 in [3]. Note that in this reference the possibility of using discontinuous interpolations and variable physical properties is taken into account, whereas here we are considering continuous interpolations and a constant μ. Note also that the convergence result obtained is optimal. The same comments as for the AG formulation regarding the regularity of the continuous solution apply in this case.

As for the AG formulation, we also have the following corollary.

Corollary 2. *Under the assumptions of Corollary 1, estimate (20) also holds for the OSGS formulation.*

Proof. This result is proved as Corollary 1, now using the $L^2(\Omega)$ and $H^1(\Omega)$ stability of the $L^2(\Omega)$-projection $P_{\mathcal{V}_h}$. □

In the case of the OSGS formulation an important simplification is possible, due to the fact that $\|P_h^{\perp}(\nabla\phi)\|_{L^2(\Omega)}$ tends to zero as $h \to 0$ at the optimal rate allowed by the FE interpolation and the smoothness of the solution. Indeed, we may consider the solution $[\boldsymbol{u}_h^*, p_h^*]$ to the following problem:

$$B_{\mathrm{OSGS}}([\boldsymbol{u}_h^*, p_h^*], [\boldsymbol{v}_h, q_h]) = (\boldsymbol{f}, \boldsymbol{v}_h) \quad \forall [\boldsymbol{v}_h, q_h] \in \mathcal{X}_h, \tag{24}$$

i.e., the problem obtained without the second term in $L_{\mathrm{OSGS}}([\boldsymbol{v}_h, q_h])$ given in (12) or, in other words, with the same forcing term as if $\boldsymbol{f}$ were divergence free. In this case, we have:

Proposition 1. *Let $[\boldsymbol{u}_h, p_h] \in \mathcal{X}_h$ be the solution of problem* (10) *with* S = OSGS *and $[\boldsymbol{u}_h^*, p_h^*] \in \mathcal{X}_h$ the solution of problem* (24)*. Then, there holds*

$$\|[\boldsymbol{u}_h - \boldsymbol{u}_h^*, p_h - p_h^*]\|_{\mathrm{OSGS}} \lesssim \frac{\ell}{\mu^{1/2}}\|\nabla\phi - P_h(\nabla\phi)\|_{L^2(\Omega)}.$$

Proof. Subtracting (10) with S = OSGS and (24) it turns out that the difference $[\boldsymbol{u}_h - \boldsymbol{u}_h^*, p_h - p_h^*] \in \mathcal{X}_h$ is solution of the problem

$$B_{\text{OSGS}}([\boldsymbol{u}_h - \boldsymbol{u}_h^*, p_h - p_h^*], [\boldsymbol{v}_h, q_h]) = \sum_K \tau_p (P_h^\perp(\nabla\phi), P_h^\perp(\nabla q_h))_K \quad \forall [\boldsymbol{v}_h, q_h] \in \mathcal{X}_h.$$

The inf-sup condition (22) implies that there exists $[\boldsymbol{v}_h, q_h] \in \mathcal{X}_h$ such that

$$\begin{aligned} \|[\boldsymbol{u}_h - \boldsymbol{u}_h^*, p_h - p_h^*]\|_{\text{OSGS}} \|[\boldsymbol{v}_h, q_h]\|_{\text{OSGS}} &\lesssim B_{\text{OSGS}}([\boldsymbol{u}_h - \boldsymbol{u}_h^*, p_h - p_h^*], [\boldsymbol{v}_h, q_h]) \\ &\lesssim \frac{\ell}{\mu^{1/2}} \|\nabla\phi - P_h(\nabla\phi)\|_{L^2(\Omega)} \|[\boldsymbol{v}_h, q_h]\|_{\text{OSGS}}, \end{aligned}$$

and the result follows. □

The importance of this result is that for the OSGS formulation we may solve the same source problem both if $\boldsymbol{f}$ is solenoidal or not, i.e., we may always solve problem (24). The solution will differ from that obtained with the fully consistent formulation (10) in a term of the same order as the FE error. In the numerical examples we shall solve (24), omitting the superscript $*$ to characterize this problem.

3.2 Eigenvalue problem

The approximation to Maxwell's EVP that we consider now is based on the stabilized FE methods introduced in the previous subsection for the source problem. For the AG formulation, the method reads: find $[\boldsymbol{u}_h, p_h] \in \mathcal{X}_h$ and $\lambda_h \in \mathbb{R}$ such that

$$\begin{aligned} \text{AG}: \qquad & B([\boldsymbol{u}_h, p_h], [\boldsymbol{v}_h, q_h]) + c_p \frac{\ell^2}{\mu} (\nabla p_h, \nabla q_h) + c_{\boldsymbol{u}} \mu \frac{h^2}{\ell^2} (\nabla \cdot \boldsymbol{u}_h, \nabla \cdot \boldsymbol{v}_h) \\ & = \lambda_h (\boldsymbol{u}_h, \boldsymbol{v}_h) + \lambda_h c_p \frac{\ell^2}{\mu} (\boldsymbol{u}_h, \nabla q_h) \qquad \forall [\boldsymbol{v}_h, q_h] \in \mathcal{X}_h, \end{aligned} \tag{25}$$

and for the OSGS formulation it reads: find $[\boldsymbol{u}_h, p_h] \in \mathcal{X}_h$ and $\lambda_h \in \mathbb{R}$ such that

$$\begin{aligned} \text{OSGS}: \qquad & B([\boldsymbol{u}_h, p_h], [\boldsymbol{v}_h, q_h]) + c_p \frac{\ell^2}{\mu} (P_h^\perp(\nabla p_h), P_h^\perp(\nabla q_h)) + c_{\boldsymbol{u}} \mu \frac{h^2}{\ell^2} (P_h^\perp(\nabla \cdot \boldsymbol{u}_h), P_h^\perp(\nabla \cdot \boldsymbol{v}_h)) \\ & = \lambda_h (\boldsymbol{u}_h, \boldsymbol{v}_h) \qquad \forall [\boldsymbol{v}_h, q_h] \in \mathcal{X}_h. \end{aligned} \tag{26}$$

Both methods are consistent when $\lambda_h \boldsymbol{u}_h$ is replaced by a non-solenoidal $\boldsymbol{f} \in L^2(\Omega)^d$. For the AG formulation, this is guaranteed by the last term in the right-hand-side, and for the OSGS formulation by the orthogonal projection applied to ∇p_h (in this case, consistency is only weak). A similar nodal based formulation was proposed in [12] with neither of the two strategies. In order to have (weak) consistency for the EVP, the authors had to multiply the term $(\nabla p_h, \nabla q_h)$ by a certain power of h, not by a fixed ℓ^2 (our AG formulation corresponds to that in [12] for the parameter $\alpha = 1$ of this reference, not allowed there).

Let us consider the matrix version of the problem. Calling U and P the arrays of nodal values of $\boldsymbol{u}_h$ and p_h, respectively, it reads

$$\begin{bmatrix} K & G \\ G^T & \tau_p L \end{bmatrix} \begin{bmatrix} U \\ P \end{bmatrix} = \lambda_h \begin{bmatrix} M & 0 \\ -\beta G^T & 0 \end{bmatrix} \begin{bmatrix} U \\ P \end{bmatrix}. \tag{27}$$

with the obvious identification of the matrices in this expression, and with $\beta = \tau_p$ for the AG formulation and $\beta = 0$ for the OSGS one. In the former case, the matrix in the right-hand-side is non-symmetric, although the discrete eigensolution converges to the continuous one (see next section). If in the AG formulation we change variables as $P = (1 + \tau_p \lambda_h) P'$ we obtain:

$$\begin{bmatrix} K & G \\ G^T & \tau_p L \end{bmatrix} \begin{bmatrix} U \\ P' \end{bmatrix} = \lambda_h \begin{bmatrix} M & -\tau_p G \\ -\tau_p G^T & -\tau_p^2 L \end{bmatrix} \begin{bmatrix} U \\ P' \end{bmatrix}.$$

This system is symmetric. It can be equivalently written as

$$\begin{bmatrix} K-\lambda_h M & (1+\tau_p\lambda_h)G \\ (1+\tau_p\lambda_h)G^T & \tau_p(1+\tau_p\lambda_h)L \end{bmatrix} \begin{bmatrix} U \\ P' \end{bmatrix} = \begin{bmatrix} 0 \\ 0 \end{bmatrix},$$

from where it follows that $\lambda_h = -1/\tau_p$ is an spurious eigenvalue associated to the change of variables. It can be filtered in several ways. However, in our numerical results we have used the original matrix from (27), despite being non-symmetric.

4 Numerical analysis of the eigenvalue problem

For the standard Galerkin method presented in Section 2, the analysis of the EVP using 2D Powell-Sabin meshes is directly presented in [11], without relying on the approximation properties of the formulation for the source problem, since this would be singular. However, for the stabilized formulations described in Section 3 we can apply the general strategy of proving convergence of eigenvalues and eigenfunctions using the results obtained for the source problem. This is what we do next. We assume in what follows that the polynomial order of the FE interpolation is higher or equal than the regularity of the solution.

As usual in the FE analysis of spectral problems [8] (see also [26]), having the existence and uniqueness of solutions to (8) and (10), we can define the solution operators $T, T_h : L^2(\Omega)^d \to L^2(\Omega)^d$ so that, for any $\boldsymbol{f} \in L^2(\Omega)^d$, $T\boldsymbol{f} = \boldsymbol{u}$ and $T_h\boldsymbol{f} = \boldsymbol{u}_h$ are the vector field components of the solutions to (8) and (10), respectively. From the convergence results of the source problems presented in the previous section, we can establish the following operator convergence

$$\|T - T_h\|_{\mathcal{L}(L^2(\Omega)^d)} \to 0 \quad \text{as } h \to 0.$$

This sets forth that the solutions of the discrete problem (25)/(26) converge to those of (2) with no spurious solutions. In particular, the convergence analysis follows along the lines of the abstract Babuška–Osborn theory [2, 8].

We recall the main results related to the approximation of the eigensolutions in the following theorems. The first theorem states the convergence of the eigensolutions and the absence of spurious modes.

Theorem 3. *Under the regularity assumptions of Corollary 1, let λ be an eigenvalue of* (5) *with multiplicity m. Then there are exactly m eigenvalues of (25)/(26), counted with their multiplicities, that converge to λ. Moreover, given a generic compact set K in the real line that does not contain any eigenvalues of* (5)*, for h small enough there are no discrete eigenvalues of* (6) *that are in K.*

Proof. From the results of Corollaries 1 and 2, we obtain that for all $\boldsymbol{f} \in L^2(\Omega)^d$

$$\|\boldsymbol{u} - \boldsymbol{u}_h\|_{L^2(\Omega)} = \|T\boldsymbol{f} - T_h\boldsymbol{f}\|_{L^2(\Omega)} \lesssim \rho(h)\|\boldsymbol{f}\|_{L^2(\Omega)},$$

with $\rho(h) \to 0$ as $h \to 0$, that is, we have the convergence in norm $\|T - T_h\|_{\mathcal{L}(L^2(\Omega)^d)} \to 0$ as h tends to zero. From the standard Babuška–Osborn theory [2], this implies the theorem. □

The second theorem states the rate of convergence of eigenvalues and eigenfunctions.

Theorem 4. *Let λ be an eigenvalue of* (5) *with multiplicity m and with an eigenspace composed of eigenfunctions $\boldsymbol{u}$ with the following regularity for some $r > 0$*

$$\begin{aligned} &\boldsymbol{u} \in H^r(\Omega), \\ &\nabla \times \boldsymbol{u} \in H^r(\Omega). \end{aligned}$$

Let us denote by λ_h^i, $i = 1, \ldots, m$, the m discrete eigenvalues corresponding to λ according to Theorem 3. Then we have the following error estimates:

$$\begin{aligned} &|\lambda - \lambda_h^i| = O(h^{2r}), \quad i = 1, \ldots, m, \\ &\hat{\delta}(E, E_h) = O(h^r), \end{aligned}$$

where E is the eigenspace associated with λ, E_h is the direct sum of the eigenspaces associated with λ_h^i, $i = 1, \dots, m$, and $\hat{\delta}$ denotes the gap between Hilbert subspaces in the energy norm.

Proof. Again, this result follows from the standard Babuška–Osborn theory [2] and the error estimates available for the source problem. □

The result about the eigenfunctions convergence can be made more explicit by interpreting the definition of gap as follows. Let $\boldsymbol{u}$ be an eigenfunction associated with λ and denote by $\boldsymbol{\phi}_h^1, \dots, \boldsymbol{\phi}_h^m$ the eigenfunctions associated with the m discrete eigenvalues converging to λ. Then there exists a linear combination $\boldsymbol{u}_h \in \operatorname{span}\{\boldsymbol{\phi}_h^1, \dots, \boldsymbol{\phi}_h^m\}$ such that

$$|||\boldsymbol{u} - \boldsymbol{u}_h||| = O(h^r),$$

where $|||\cdot|||$ means $\|\cdot\|_{\mathrm{AG}}$ or $\|\cdot\|_{\mathrm{OSGS}}$ for the AG or OSGS formulation, respectively.

5 Numerical results

As a first numerical example, we present a simple experiment where Assumption 1 holds. The considered test is quite general and suggests that Assumption 1 is valid in a broad range of situations, if not all. We present then three numerical tests for the approximation of the Maxwell EVP with $\mu = 1$ on three different domains, namely, a square domain, a flipped L-shape domain, and a cracked square domain, all of them in 2D. We consider the square domain for validation purposes, since the analytical solutions are available. The L-shaped domain consists of non-smooth solutions and hence it is a standard benchmark to test the methodology for singular problems. The cracked square domain contains a slit which makes it a distinguished candidate for serving as a challenging task with a solution that exhibits a strong singularity.

The standard Galerkin method (4), from now on SG, and the stabilized (AG and OSGS) formulations (25)/(26) are implemented using criss-cross (CC) and Powell-Sabin (PS) meshes. We have also considered a sequence of uniform right diagonal meshes for a distinct case (see Section 5.2). The CC mesh sequences are used as it is well known that the gradients are well represented by the given interpolations, although there is no theoretical support for their performance in the Maxwell problem. In fact, in [4] it was shown through numerical experiments that they provide good results for the source problem using the AG formulation, and here we will test these meshes for the EVP. The PS meshes are chosen due to their convergence results as we have already stated. For all the unknowns we have employed equal order (for both $\boldsymbol{u}_h$ and p_h) of linear (P_1) and quadratic (P_2) interpolations, even though much of the focus is placed on the results obtained from the former.

All the results we present below have been obtained by means of computer programs written by us using Matlab. The eigenvalues are obtained by its built-in function *eigs* that calculates a subset of eigensolutions of a (generalized) matrix eigenvalue system. For the SG formulation, the discrete spectrum consists of a number of zeros; the discrete frequencies approximating zero are eliminated to present the first nonzero values. The correctness of these approximations is verified using Matlab's *eig* function calculating all of the discrete eigenvalues for sizes that fit well in memory. However, the restriction of eliminating a huge number of (machine) zeros from the approximate spectrum is alleviated when considering the stabilized formulations which, by construction, result in strictly positive eigenvalues for all the cases considered.

The values of the algebraic constants in the definition of the stabilization parameters, $c_{\boldsymbol{u}}$ and c_p, and the characteristic length ℓ can be taken in a wide range, influencing the accuracy while preserving similar convergence behaviors. The specific values taken for the simulations are given for each test domain individually. We denote by N the number of divisions in each direction for the square domain, and the number of division in one of the short edges for the L-shaped domain. The tables we provide in the sequel list the approximated eigenvalues together with their rates of convergence towards the reference values indicated in parentheses.

Regarding the boundary conditions, we have considered $\boldsymbol{n} \times \boldsymbol{u}_h = \boldsymbol{0}$ on the boundaries. At convex corners of the computational domain we have prescribed both components of $\boldsymbol{u}_h$ to zero. However, the situation is more delicate at re-entrant corners; the way to impose boundary conditions there is explained for the two examples in which this situation is found. It is important to point out here that the theoretical results in view of Theorem 4 are

in correspondence with the strictly conforming approximations where both components are forced to be zero at all boundary corners. On the other hand, the exact solutions of the problems we consider in the sequel that are defined on domains with re-entrant corners have incompatible (with these boundary conditions) behaviors on these nodes, and only the tangential component is zero while the solution is singular at the re-entrant corner. For this reason, in the numerical tests for the singular cases already mentioned we investigate numerically different ways of imposing the boundary conditions aiming at leaving more flexibility to the solution which can be considered solely to improve the results.

5.1 Testing Assumption 1

In this first example we test the possible validity of Assumption 1. For that, we consider a sequence of uniform FE meshes of size h that discretize the domain $\Omega_1 =]0, \pi[^2$ (see Figure 2). The mesh-dependent forcing term is of the form $\boldsymbol{f}_h(x, y) = \nabla\phi_h(x, y)$, with $\phi_h(x, y) = \phi_0\varphi_h(x)\varphi_h(y)$. The function $\varphi_h(z)$ takes the value one at the central node, with $z = \pi/2$, and zero at the nodes with $z \leq \pi/2 - h$ or $z \geq \pi/2 + h$, being piecewise linear and continuous. For PS meshes, h corresponds to the size of the macro-element. The resulting function $\phi_h(x, y)$ constructed this way will be bilinear, and different from zero only in a patch of elements around the central node. Observe that $\|\nabla(\varphi_h(x)\varphi_h(y))\|_{L^2(\Omega)}$ is bounded independently of h ($\nabla\varphi_h(x)$ is piecewise constant behaving as h^{-1} and the support of $\varphi_h(x)\varphi_h(y)$ has measure of order h^2). We choose the constant ϕ_0 such that $\|\nabla\phi_h(x, y)\|_{L^2(\Omega)} = 1$. Hence, we can conclude that $\|\phi_h(x, y)\|_{H^1(\Omega)}$ is uniformly bounded (thanks to the Poincaré inequality), and consequently there exists the (weak) limit $\phi^* \in H^1_0(\Omega)$ of ϕ_h as $h \to 0$. The limiting solution to the problem we consider is thus $\boldsymbol{u} = \boldsymbol{0}$ and $p = \phi^*$. The surface plots of $p(h)$ constructed in this way on a PS mesh where $N = 32$ and its corresponding approximation using the AG formulation p_h are shown in Figure 1.

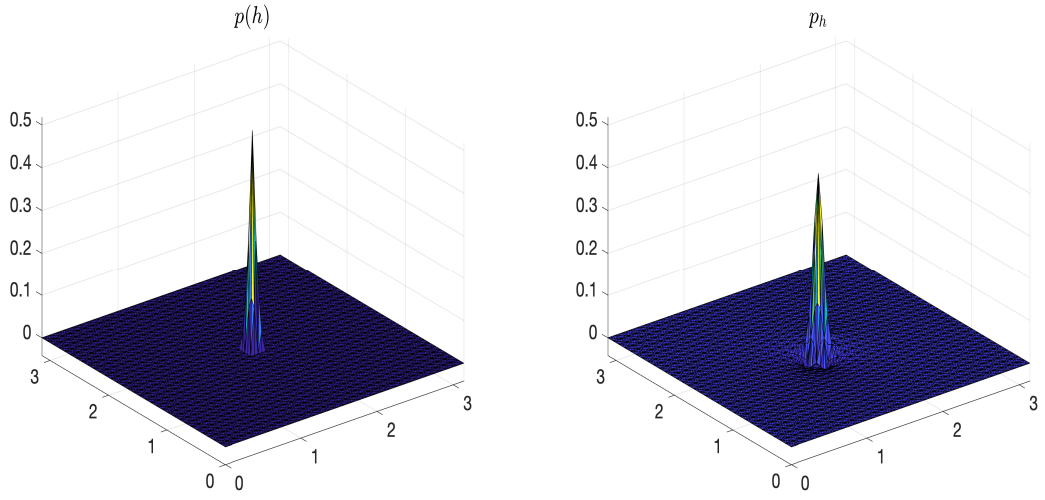

Fig. 1: Surface plots of $p(h)$ and p_h obtained using the AG formulation on PS mesh where $N = 32$.

In order to investigate the anticipated behavior, we compute the $L^2(\Omega)$-norms of the numerical errors $\|\boldsymbol{u}_h\|$, $\|\nabla \times \boldsymbol{u}_h\|$, $\|p_h - p(h)\|$, and $\|\nabla(p_h - p(h))\|$, together with their computed convergence rates as h tends to zero on uniform diagonal and PS meshes. The results are presented in Tables 1 and 2 using the OSGS and AG formulations,

Tab. 1: Errors and rates of convergence (in brackets) on different triangulations: OSGS formulation.

Triangulation	h	$\|\boldsymbol{u}_h\|$	$\|\nabla \times \boldsymbol{u}_h\|$	$\|p_h - p(h)\|$	$\|\nabla(p_h - p(h))\|$
Uniform diagonal	**0.5554**	**1.01e-01**	**1.05e-01**	**1.12e+00**	**1.11e+00**
	0.2777	**5.12e-02 (0.98)**	**5.47e-02 (0.94)**	**1.42e+00 (-0.34)**	**1.34e+00 (-0.27)**
	0.1388	**2.57e-02 (0.99)**	**2.86e-02 (0.93)**	**1.40e+00 (0.02)**	**1.24e+00 (0.12)**
	0.0694	**1.30e-02 (0.99)**	**1.62e-02 (0.82)**	**1.25e+00 (0.16)**	**1.03e+00 (0.26)**
	0.0347	**6.52e-03 (1.00)**	**9.20e-03 (0.82)**	**1.20e+00 (0.06)**	**9.50e-01 (0.12)**
Powell-Sabin	**0.6011**	**1.07e-01**	**1.22e-01**	**4.51e-01**	**5.71e-01**
	0.3006	**5.60e-02 (0.93)**	**6.82e-02 (0.83)**	**4.86e-01 (-0.11)**	**5.58e-01 (0.03)**
	0.1503	**2.84e-02 (0.98)**	**3.71e-02 (0.88)**	**5.21e-01 (-0.10)**	**5.59e-01 (-0.00)**
	0.0751	**1.42e-02 (0.99)**	**2.00e-02 (0.90)**	**5.53e-01 (-0.09)**	**5.59e-01 (0.00)**
	0.0376	**7.12e-03 (1.00)**	**1.06e-02 (0.91)**	**5.84e-01 (-0.08)**	**5.58e-01 (0.00)**

Tab. 2: Errors and rates of convergence (in brackets) on different triangulations: AG formulation.

Triangulation	h	$\|\boldsymbol{u}_h\|$	$\|\nabla \times \boldsymbol{u}_h\|$	$\|p_h - p(h)\|$	$\|\nabla(p_h - p(h))\|$
Uniform diagonal	**0.5554**	**1.01e-01**	**1.05e-01**	**8.14e-01**	**7.85e-01**
	0.2777	**5.12e-02 (0.98)**	**5.47e-02 (0.94)**	**8.92e-01 (-0.13)**	**8.00e-01 (-0.03)**
	0.1388	**2.57e-02 (0.99)**	**2.86e-02 (0.94)**	**9.82e-01 (-0.14)**	**8.07e-01 (-0.01)**
	0.0694	**1.30e-02 (0.99)**	**1.62e-02 (0.82)**	**1.04e+00 (-0.08)**	**8.03e-01 (0.01)**
	0.0347	**6.52e-03 (1.00)**	**9.19e-03 (0.82)**	**1.07e+00 (-0.04)**	**7.97e-01 (0.01)**
Powell-Sabin	**0.6011**	**1.07e-01**	**1.22e-01**	**4.17e-01**	**5.16e-01**
	0.3006	**5.60e-02 (0.93)**	**6.82e-02 (0.83)**	**4.52e-01 (-0.11)**	**5.21e-01 (-0.02)**
	0.1503	**2.84e-02 (0.98)**	**3.71e-02 (0.88)**	**4.89e-01 (-0.11)**	**5.22e-01 (-0.00)**
	0.0751	**1.42e-02 (0.99)**	**2.00e-02 (0.90)**	**5.24e-01 (-0.10)**	**5.22e-01 (-0.00)**
	0.0376	**7.12e-03 (1.00)**	**1.06e-02 (0.91)**	**5.56e-01 (-0.09)**	**5.23e-01 (-0.00)**

respectively. These results allow us to deduce the followings:

$$
\begin{aligned}
&\|\boldsymbol{u}_h\| = \|\boldsymbol{u} - \boldsymbol{u}_h\| = \|\boldsymbol{u}(h) - \boldsymbol{u}_h\| = O(h),\\
&\|\nabla \times \boldsymbol{u}_h\| = \|\nabla \times (\boldsymbol{u} - \boldsymbol{u}_h)\| = \|\nabla \times (\boldsymbol{u}(h) - \boldsymbol{u}_h)\| = O(h),\\
&\|p(h) - p_h\| = O(1),\\
&\|\nabla(p(h) - p_h)\| = O(1).
\end{aligned}
$$

From these, we can establish the inequality $\|\boldsymbol{u} - \boldsymbol{u}_h\| \lesssim h\|p(h) - p_h\|$. Therefore, we can conclude that Assumption 1 indeed holds (with $s = 1$) for this particular example. It is also relevant to remark that this is true both for PS meshes and for uniform P_1 meshes. Naturally, these results do not imply the validity of Assumption 1 in general, but they constitute a good indication that it is likely to hold under quite general assumptions.

5.2 The square domain

For the first numerical test, we consider an approximation of Maxwell's EVP on the square Ω_1. In this case, the exact solutions are known, and the eigenvalues are given as $\lambda_{m,n} = m^2 + n^2$, where $m, n = 0, 1, \ldots$, and $m + n \neq 0$. It is well known that SG formulations may result in unphysical values even for problems with smooth solutions unless certain conditions on the mesh topology are satisfied. More specifically, adequate gradients of the solution should be provided by the discrete space to ensure that the zero frequency is exactly approximated by vanishing discrete eigenvalues. An example to the existence of spurious eigenvalues has already been presented in [8], in which the SG scheme for the discretization of the problem on Ω_1 has been used with a sequence of CC meshes. Besides realization of this issue, in order to compare the SG formulation with the stabilized ones on the same meshes, we compute the corresponding eigenvalues using CC meshes and PS meshes, and list the results in the following. Table 3 lists the first 17 approximate eigenvalues using the SG formulation and P_1 elements on CC meshes. As it is evident from the negative rates, some listed limit values are spurious and are not associated with any true eigenvalues, even though a

number of selected ones show a good convergence. This pathology, which occurs even in the case of smooth solutions, is already known (see [8]) and it is the main motivation for the need of stabilization strategies implemented for nodal elements.

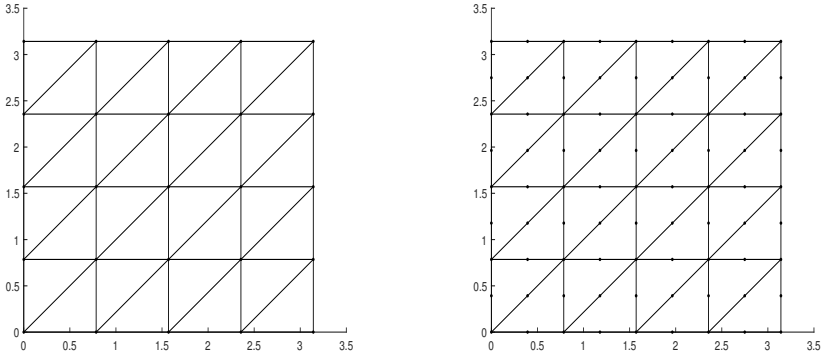

Fig. 2: Uniform meshes and node distributions used for P_1 (left) and P_2 (right) interpolations on Ω_1.

Tab. 3: The first 17 eigenvalues on Ω_1 using the SG formulation and P_1 elements on CC meshes.

Exact	Computed				
	$N = 5$	$N = 10$	$N = 15$	$N = 20$	$N = 25$
1.0000	**1.0109**	**1.0027 (2.0)**	**1.0012 (2.0)**	**1.0007 (2.0)**	**1.0004 (2.0)**
1.0000	**1.0109**	**1.0027 (2.0)**	**1.0012 (2.0)**	**1.0007 (2.0)**	**1.0004 (2.0)**
2.0000	**2.0437**	**2.0110 (2.0)**	**2.0049 (2.0)**	**2.0027 (2.0)**	**2.0018 (2.0)**
4.0000	**4.1719**	**4.0437 (2.0)**	**4.0195 (2.0)**	**4.0110 (2.0)**	**4.0070 (2.0)**
4.0000	**4.1719**	**4.0437 (2.0)**	**4.0195 (2.0)**	**4.0110 (2.0)**	**4.0070 (2.0)**
5.0000	**5.2657**	**5.0683 (2.0)**	**5.0304 (2.0)**	**5.0171 (2.0)**	**5.0110 (2.0)**
5.0000	**5.2657**	**5.0683 (2.0)**	**5.0304 (2.0)**	**5.0171 (2.0)**	**5.0110 (2.0)**
8.0000	**5.7988**	**5.9507 (0.1)**	**5.9781 (0.0)**	**5.9877 (0.0)**	**5.9921 (0.0)**
9.0000	**8.6504**	**8.1746 (-1.2)**	**8.0779 (-0.3)**	**8.0438 (-0.1)**	**8.0281 (-0.1)**
9.0000	**9.8403**	**9.2197 (1.9)**	**9.0982 (2.0)**	**9.0554 (2.0)**	**9.0355 (2.0)**
10.0000	**9.8403**	**9.2197 (-2.3)**	**9.0982 (-0.4)**	**9.0554 (-0.2)**	**9.0355 (-0.1)**
10.0000	**10.9783**	**10.2710 (1.9)**	**10.1213 (2.0)**	**10.0684 (2.0)**	**10.0438 (2.0)**
13.0000	**10.9783**	**10.2710 (-0.4)**	**10.1213 (-0.1)**	**10.0684 (-0.1)**	**10.0438 (-0.0)**
13.0000	**12.5826**	**13.4573 (-0.1)**	**13.2052 (2.0)**	**13.1156 (2.0)**	**13.0741 (2.0)**
16.0000	**12.5826**	**13.4573 (0.4)**	**13.2052 (-0.2)**	**13.1156 (-0.1)**	**13.0741 (-0.1)**
16.0000	**14.3233**	**14.3101 (-0.0)**	**14.6791 (0.6)**	**14.8163 (0.4)**	**14.8814 (0.3)**
17.0000	**14.3233**	**14.3101 (-0.0)**	**14.6791 (0.4)**	**14.8163 (0.2)**	**14.8814 (0.1)**

Tables 4 and 5 respectively list the analogous results obtained from the AG and OSGS formulations. These are obtained taking $\ell = 0.1$ and $c_{\boldsymbol{u}} = 0.1$, when $\tau_p = 1$. The significant role in the relief of the aforementioned pathology can easily be evidenced from the correct values of the eigenvalues, and with the expected rates of convergence. Both the AG and OSGS schemes yield very similar convergence behaviors noting that the latter achieves a slightly more accuracy than the former for the same algorithmic constants.

Regarding the SG formulation, having arrived at the important conclusion that PS meshes should be used due to the potential risk of obtaining spurious eigenvalues otherwise, we present the results obtained from PS meshes when considering formulation (4) in what follows. We tabulate the first 17 eigenvalues obtained using this formulation on PS meshes in Table 6 to numerically validate its convergence characteristics.

Before closing this subsection, let us emphasize that both stabilized formulations produce exceptional results in the case of smooth solutions independent of the mesh types we have tested in this work. To further corroborate

Tab. 4: The first 17 eigenvalues on Ω_1 using the AG formulation and P_1 elements on CC meshes.

Exact	Computed				
	$N=5$	$N=10$	$N=15$	$N=20$	$N=25$
1.0000	1.0287	1.0055 (2.4)	1.0020 (2.5)	1.0010 (2.5)	1.0006 (2.4)
1.0000	1.0287	1.0055 (2.4)	1.0020 (2.5)	1.0010 (2.5)	1.0006 (2.4)
2.0000	2.0624	2.0138 (2.2)	2.0056 (2.2)	2.0030 (2.2)	2.0019 (2.1)
4.0000	4.4705	4.0879 (2.4)	4.0314 (2.5)	4.0153 (2.5)	4.0089 (2.4)
4.0000	4.4705	4.0879 (2.4)	4.0314 (2.5)	4.0153 (2.5)	4.0089 (2.4)
5.0000	5.5321	5.1049 (2.3)	5.0402 (2.4)	5.0207 (2.3)	5.0125 (2.2)
5.0000	5.5321	5.1049 (2.3)	5.0402 (2.4)	5.0207 (2.3)	5.0125 (2.2)
8.0000	9.0402	8.2229 (2.2)	8.0904 (2.2)	8.0483 (2.2)	8.0300 (2.1)
9.0000	11.3842	9.4479 (2.4)	9.1593 (2.6)	9.0775 (2.5)	9.0452 (2.4)
9.0000	11.3842	9.4479 (2.4)	9.1593 (2.6)	9.0775 (2.5)	9.0452 (2.4)
10.0000	12.5909	10.4803 (2.4)	10.1766 (2.5)	10.0884 (2.4)	10.0526 (2.3)
10.0000	12.5909	10.4803 (2.4)	10.1766 (2.5)	10.0884 (2.4)	10.0526 (2.3)
13.0000	16.2807	13.6459 (2.3)	13.2532 (2.3)	13.1327 (2.2)	13.0815 (2.2)
13.0000	16.2807	13.6459 (2.3)	13.2532 (2.3)	13.1327 (2.2)	13.0815 (2.2)
16.0000	22.4531	17.4246 (2.2)	16.5042 (2.6)	16.2450 (2.5)	16.1428 (2.4)
16.0000	22.4531	17.4246 (2.2)	16.5042 (2.6)	16.2450 (2.5)	16.1428 (2.4)
17.0000	23.3681	18.4812 (2.1)	17.5335 (2.5)	17.2636 (2.5)	17.1555 (2.4)

Tab. 5: The first 17 eigenvalues on Ω_1 using the OSGS formulation and P_1 elements on CC meshes.

Exact	Computed				
	$N=5$	$N=10$	$N=15$	$N=20$	$N=25$
1.0000	1.0279	1.0053 (2.4)	1.0019 (2.5)	1.0009 (2.5)	1.0006 (2.4)
1.0000	1.0279	1.0053 (2.4)	1.0019 (2.5)	1.0009 (2.5)	1.0006 (2.4)
2.0000	2.0606	2.0135 (2.2)	2.0056 (2.2)	2.0030 (2.2)	2.0019 (2.1)
4.0000	4.4574	4.0858 (2.4)	4.0309 (2.5)	4.0152 (2.5)	4.0089 (2.4)
4.0000	4.4589	4.0858 (2.4)	4.0309 (2.5)	4.0152 (2.5)	4.0089 (2.4)
5.0000	5.5008	5.1007 (2.3)	5.0393 (2.3)	5.0204 (2.3)	5.0124 (2.2)
5.0000	5.5008	5.1007 (2.3)	5.0393 (2.3)	5.0204 (2.3)	5.0124 (2.2)
8.0000	9.0117	8.2181 (2.2)	8.0894 (2.2)	8.0480 (2.2)	8.0299 (2.1)
9.0000	11.3376	9.4377 (2.4)	9.1569 (2.5)	9.0768 (2.5)	9.0449 (2.4)
9.0000	11.3376	9.4377 (2.4)	9.1569 (2.5)	9.0768 (2.5)	9.0449 (2.4)
10.0000	12.3916	10.4553 (2.4)	10.1713 (2.4)	10.0869 (2.4)	10.0520 (2.3)
10.0000	12.4487	10.4560 (2.4)	10.1714 (2.4)	10.0869 (2.4)	10.0520 (2.3)
13.0000	16.0939	13.6212 (2.3)	13.2482 (2.3)	13.1313 (2.2)	13.0810 (2.2)
13.0000	16.0939	13.6212 (2.3)	13.2482 (2.3)	13.1313 (2.2)	13.0810 (2.2)
16.0000	22.3404	17.3939 (2.2)	16.4968 (2.5)	16.2428 (2.5)	16.1420 (2.4)
16.0000	22.4359	17.3959 (2.2)	16.4970 (2.5)	16.2428 (2.5)	16.1420 (2.4)
17.0000	23.2581	18.4019 (2.2)	17.5162 (2.5)	17.2585 (2.4)	17.1537 (2.3)

this, in Tables 7 and 8 we list the approximations to the first 10 eigenvalues using respectively P_1 and P_2 elements on standard uniform (right diagonal) meshes, a sample of which is shown in Figure 2. These results are obtained from the OSGS formulation; however, they are very similar to the ones obtained from the AG formulation, which are not included for brevity. We can easily infer from these results that the stabilization achieves a double order of convergence without any spurious value, as it is anticipated from the theory.

5.3 The L-shaped domain

In this subsection we want to examine a widely considered test case, e.g., in [12, 14, 19, 20], that is an L-shaped domain with a re-entrant corner, defined by $\Omega_2 =]-1,1[^2 \setminus \{[0,1] \times [-1,0]\}$. The CC and PS discretizations of this domain with $N = 5$ are shown in Figure 3. All of the reported values computed by a stabilized formulation

Tab. 6: The first 17 eigenvalues on Ω_1 using the SG formulation and P_1 elements on PS meshes.

Exact	Computed				
	$N = 5$	$N = 10$	$N = 15$	$N = 20$	$N = 25$
1.0000	**1.0029**	**1.0007 (2.0)**	**1.0003 (2.0)**	**1.0002 (2.0)**	**1.0001 (2.0)**
1.0000	**1.0072**	**1.0018 (2.0)**	**1.0008 (2.0)**	**1.0005 (2.0)**	**1.0003 (2.0)**
2.0000	**2.0197**	**2.0051 (2.0)**	**2.0023 (2.0)**	**2.0013 (2.0)**	**2.0008 (2.0)**
4.0000	**4.0792**	**4.0203 (2.0)**	**4.0090 (2.0)**	**4.0051 (2.0)**	**4.0033 (2.0)**
4.0000	**4.0796**	**4.0203 (2.0)**	**4.0090 (2.0)**	**4.0051 (2.0)**	**4.0033 (2.0)**
5.0000	**5.0772**	**5.0212 (1.9)**	**5.0095 (2.0)**	**5.0054 (2.0)**	**5.0035 (2.0)**
5.0000	**5.1596**	**5.0416 (1.9)**	**5.0186 (2.0)**	**5.0105 (2.0)**	**5.0067 (2.0)**
8.0000	**8.2651**	**8.0786 (1.8)**	**8.0357 (1.9)**	**8.0202 (2.0)**	**8.0130 (2.0)**
9.0000	**9.3628**	**9.0968 (1.9)**	**9.0434 (2.0)**	**9.0245 (2.0)**	**9.0157 (2.0)**
9.0000	**9.4040**	**9.1067 (1.9)**	**9.0478 (2.0)**	**9.0269 (2.0)**	**9.0173 (2.0)**
10.0000	**10.4348**	**10.1242 (1.8)**	**10.0560 (2.0)**	**10.0317 (2.0)**	**10.0203 (2.0)**
10.0000	**10.4494**	**10.1251 (1.8)**	**10.0562 (2.0)**	**10.0317 (2.0)**	**10.0203 (2.0)**
13.0000	**13.4436**	**13.1522 (1.5)**	**13.0699 (1.9)**	**13.0397 (2.0)**	**13.0255 (2.0)**
13.0000	**13.7494**	**13.2576 (1.5)**	**13.1178 (1.9)**	**13.0668 (2.0)**	**13.0429 (2.0)**
16.0000	**17.0734**	**16.3173 (1.8)**	**16.1433 (2.0)**	**16.0810 (2.0)**	**16.0520 (2.0)**
16.0000	**17.0912**	**16.3176 (1.8)**	**16.1434 (2.0)**	**16.0810 (2.0)**	**16.0520 (2.0)**
17.0000	**17.9694**	**17.3329 (1.5)**	**17.1518 (1.9)**	**17.0860 (2.0)**	**17.0552 (2.0)**

Tab. 7: The first 10 eigenvalues on Ω_1 using the OSGS formulation and P_1 elements on the uniform mesh shown in Figure 2.

Exact	Computed				
	$N = 20$	$N = 25$	$N = 30$	$N = 35$	$N = 40$
1.0000	**1.0021**	**1.0013 (2.0)**	**1.0009 (2.0)**	**1.0007 (2.0)**	**1.0005 (2.0)**
1.0000	**1.0021**	**1.0013 (2.0)**	**1.0009 (2.0)**	**1.0007 (2.0)**	**1.0005 (2.0)**
2.0000	**2.0073**	**2.0044 (2.3)**	**2.0030 (2.2)**	**2.0021 (2.1)**	**2.0016 (2.1)**
4.0000	**4.0329**	**4.0210 (2.0)**	**4.0146 (2.0)**	**4.0107 (2.0)**	**4.0082 (2.0)**
4.0000	**4.0329**	**4.0211 (2.0)**	**4.0146 (2.0)**	**4.0107 (2.0)**	**4.0082 (2.0)**
5.0000	**5.0385**	**5.0239 (2.1)**	**5.0164 (2.1)**	**5.0119 (2.1)**	**5.0091 (2.0)**
5.0000	**5.0572**	**5.0351 (2.2)**	**5.0239 (2.1)**	**5.0173 (2.1)**	**5.0131 (2.1)**
8.0000	**8.1167**	**8.0706 (2.3)**	**8.0475 (2.2)**	**8.0342 (2.1)**	**8.0258 (2.1)**
9.0000	**9.1666**	**9.1065 (2.0)**	**9.0739 (2.0)**	**9.0543 (2.0)**	**9.0416 (2.0)**
9.0000	**9.1667**	**9.1066 (2.0)**	**9.0740 (2.0)**	**9.0543 (2.0)**	**9.0416 (2.0)**

concerning this domain are obtained using $\ell = 0.3$, $c_{\boldsymbol{u}} = 0.3$, and $\tau_p = 1$. In the numerical results, we use the reference values taken from [19] for comparison.

It is known that the first eigenvalue is the most critical when an approximation is considered, as it corresponds to the eigenfunction that has the lowest regularity, being it in $(H^{2/3-\epsilon}(\Omega))^2$ for any $\epsilon > 0$. When nodal elements are used, the existence of such a singularity manifests itself in the drastic change of the results depending on the way the normal vector is treated at the re-entrant corner in the process of boundary condition imposition. To realize and examine this computationally, we have tried three alternative ways of handling the components of the unknown vector field at the re-entrant corner of the enclosure; this is an issue in the case of nodal-based formulations. The first two alternatives are to force both of the components to vanish at the corner, or to leave them free at that node. The third one consists of assigning a fictitious normal vector due to the geometrical convenience. Specifically, this last strategy depends on assuming that the normal is the bisector of this corner, and imposing the boundary condition $\boldsymbol{n} \times \boldsymbol{u}_h = \boldsymbol{0}$ in the following way. The tangent component of $\boldsymbol{u}$ is 0, and $\boldsymbol{u}$ has to follow the normal $\boldsymbol{n}$. In this way, if we write $\boldsymbol{u} = [u_1, u_2]^{\mathsf{T}}$, we impose the condition $u_2 = -u_1$, and solve for u_1.

We present the corresponding results obtained using PS meshes with the SG formulation in Table 9 and the OSGS formulation in Table 10. These results clearly show that alternative strategies for enforcing the boundary condition

Tab. 8: The first 10 eigenvalues on Ω_1 using the OSGS formulation and P_2 elements on the uniform mesh shown in Figure 2.

Exact	Computed				
	$N = 20$	$N = 25$	$N = 30$	$N = 35$	$N = 40$
1.0000	**1.0000**	**1.0000 (4.0)**	**1.0000 (4.0)**	**1.0000 (4.0)**	**1.0000 (4.0)**
1.0000	**1.0000**	**1.0000 (4.0)**	**1.0000 (4.0)**	**1.0000 (4.0)**	**1.0000 (4.0)**
2.0000	**2.0000**	**2.0000 (4.1)**	**2.0000 (4.1)**	**2.0000 (4.1)**	**2.0000 (4.1)**
4.0000	**4.0001**	**4.0000 (4.0)**	**4.0000 (4.0)**	**4.0000 (4.0)**	**4.0000 (4.0)**
4.0000	**4.0001**	**4.0000 (4.0)**	**4.0000 (4.0)**	**4.0000 (4.0)**	**4.0000 (4.0)**
5.0000	**5.0001**	**5.0000 (4.0)**	**5.0000 (4.0)**	**5.0000 (4.0)**	**5.0000 (4.0)**
5.0000	**5.0001**	**5.0000 (4.1)**	**5.0000 (4.0)**	**5.0000 (4.0)**	**5.0000 (4.0)**
8.0000	**8.0004**	**8.0002 (4.1)**	**8.0001 (4.1)**	**8.0000 (4.1)**	**8.0000 (4.0)**
9.0000	**9.0006**	**9.0002 (4.0)**	**9.0001 (4.0)**	**9.0001 (4.0)**	**9.0000 (4.0)**
9.0000	**9.0006**	**9.0002 (4.0)**	**9.0001 (4.0)**	**9.0001 (4.0)**	**9.0000 (4.0)**

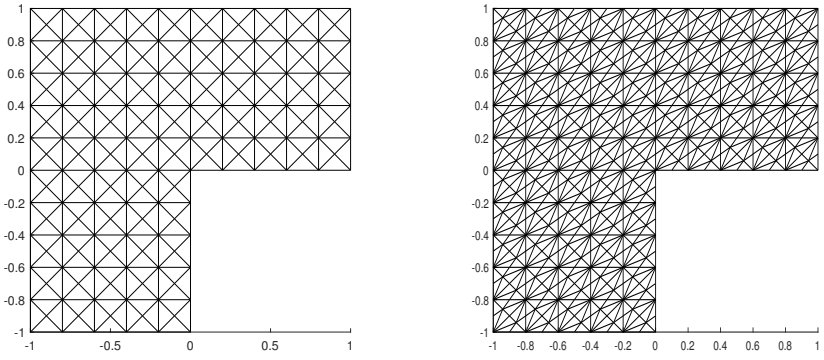

Fig. 3: A sample triangulation of the L-shaped domain with CC (left) and PS (right) mesh, where $N = 5$.

at the re-entrant corner of the enclosure result in significantly different approximations in the first eigenvalue. The most remarkable deduction emanating from these tables is the influence of the treatment of the re-entrant corner with or without stabilization. It can be easily seen that leaving the components free at the corner lead to accurate results in the case of stabilization while it is not convenient at all for the SG formulation. The bisector normal strategy seems to work well for all of the formulations. Let us note here that despite of this difference, we have observed that the convergence properties are very similar. It is also of significant importance to note once again that the results obtained from the SG formulation seem to be more accurate than the ones obtained from the stabilized formulations. On the other hand, it is always possible to increase the accuracy in the latter schemes by manipulating the stabilization parameters, even though this has not been the main aim of this research.

In the light of these investigations, the approximations for this domain case using PS meshes and following the bisector normal strategy are listed in Tables 11, 12, and 13 for the SG, AG, and OSGS formulations, respectively. From these tables we can see that the convergences rates are the ones expected from the theory. Specifically, there are no spurious values encountered in any of the formulations considered. The smallest rate of convergence is observed for the first eigenvalue, whose corresponding eigenfunction has the lowest regularity. Moreover, the OSGS formulation seems to be slightly more accurate for the fundamental eigenvalue in comparison with the AG formulation; when implemented using the same set of stabilization parameters.

The plots of the components of the fundamental eigenfunction, that is associated with the minimum eigenvalue, obtained using the OSGS formulation on the PS mesh where $N = 25$, are presented in Figure 4. The approximations that are obtained from the bisector normal strategy show well the singularity near the re-entrant corner, corroborating the pattern of the eigenfunction that can be expected.

Tab. 9: The first 10 nonzero eigenvalues on Ω_2 using PS mesh and the SG formulation, $N = 9$.

bisector normal	$u_1 = u_2 = 0$	u_1, u_2 free
1.4876	1.4435	0.1181
3.5348	3.5348	1.4876
9.8829	9.8829	3.5351
9.8873	9.8873	9.8829
11.4032	11.4032	10.3660
12.6424	12.4952	11.4038
19.8006	19.8006	12.6424
21.5789	21.2304	20.3093
23.4182	23.4182	21.5789
28.7328	28.3622	23.4234

Tab. 10: The first 10 nonzero eigenvalues on Ω_2 using PS mesh and the OSGS formulation, $N = 9$.

bisector normal	$u_1 = u_2 = 0$	u_1, u_2 free
1.6252	2.2203	1.6252
3.5517	3.5517	3.5371
9.8836	9.8836	9.7725
9.8879	9.8879	9.8836
11.4116	11.4116	11.4058
12.6789	12.8182	12.6789
19.8034	19.8034	19.4922
21.5959	21.6729	21.5959
23.4449	23.4449	23.4287
28.5389	28.5389	28.5380

Tab. 11: The first 5 eigenvalues on Ω_2 using the SG formulation and P_1 elements on PS meshes (bisector normal).

Ref.	Computed				
	$N = 5$	$N = 10$	$N = 15$	$N = 20$	$N = 25$
1.4756	1.5024	1.4860 (1.4)	1.4816 (1.4)	1.4797 (1.4)	1.4786 (1.3)
3.5340	3.5351	3.5347 (0.7)	3.5344 (1.5)	3.5342 (1.7)	3.5342 (1.7)
9.8696	9.9124	9.8804 (2.0)	9.8744 (2.0)	9.8723 (2.0)	9.8713 (2.0)
9.8696	9.9267	9.8839 (2.0)	9.8760 (2.0)	9.8732 (2.0)	9.8719 (2.0)
11.3895	11.4314	11.4007 (1.9)	11.3946 (1.9)	11.3924 (2.0)	11.3913 (2.0)

Tab. 12: The first 5 eigenvalues on Ω_2 using the AG formulation and P_1 elements on PS meshes (bisector normal).

Ref.	Computed				
	$N = 5$	$N = 10$	$N = 15$	$N = 20$	$N = 25$
1.4756	1.6945	1.5635 (1.3)	1.5268 (1.3)	1.5105 (1.3)	1.5015 (1.3)
3.5340	3.5712	3.5406 (2.5)	3.5364 (2.5)	3.5352 (2.5)	3.5347 (2.5)
9.8696	9.9175	9.8807 (2.1)	9.8745 (2.0)	9.8723 (2.0)	9.8713 (2.0)
9.8696	9.9315	9.8842 (2.1)	9.8760 (2.0)	9.8732 (2.0)	9.8719 (2.0)
11.3895	11.4583	11.4043 (2.2)	11.3957 (2.1)	11.3929 (2.1)	11.3916 (2.1)

As a last illustration for this problem domain, we approximate the first 5 eigenvalues using the OSGS stabilized formulation on CC meshes. We list the results in Tables 14 and 15 for P_1 and P_2 elements, respectively. All the eigenvalues listed are approximated correctly, and the convergence rates are as expected. Note the unchanged rate in the

Tab. 13: The first 5 eigenvalues on Ω_2 using the OSGS formulation and P_1 elements on PS meshes (bisector normal).

Ref.	Computed				
	$N = 5$	$N = 10$	$N = 15$	$N = 20$	$N = 25$
1.4756	**1.6667**	**1.5556 (1.3)**	**1.5228 (1.3)**	**1.5079 (1.3)**	**1.4996 (1.3)**
3.5340	**3.5802**	**3.5424 (2.5)**	**3.5371 (2.5)**	**3.5355 (2.5)**	**3.5349 (2.5)**
9.8696	**9.9170**	**9.8807 (2.1)**	**9.8745 (2.0)**	**9.8723 (2.0)**	**9.8713 (2.0)**
9.8696	**9.9307**	**9.8842 (2.1)**	**9.8760 (2.0)**	**9.8732 (2.0)**	**9.8719 (2.0)**
11.3895	**11.4573**	**11.4043 (2.2)**	**11.3958 (2.1)**	**11.3929 (2.1)**	**11.3916 (2.1)**

Tab. 14: The first 5 eigenvalues on Ω_2 using the OSGS formulation and P_1 elements on CC meshes.

Ref.	Computed				
	$N = 5$	$N = 10$	$N = 15$	$N = 20$	$N = 25$
1.4756	**1.6350**	**1.5391 (1.3)**	**1.5126 (1.3)**	**1.5008 (1.3)**	**1.4943 (1.3)**
3.5340	**3.6248**	**3.5520 (2.3)**	**3.5407 (2.4)**	**3.5374 (2.4)**	**3.5360 (2.4)**
9.8696	**10.0023**	**9.8985 (2.2)**	**9.8820 (2.1)**	**9.8765 (2.0)**	**9.8740 (2.0)**
9.8696	**10.0032**	**9.8985 (2.2)**	**9.8820 (2.1)**	**9.8765 (2.0)**	**9.8740 (2.0)**
11.3895	**11.5771**	**11.4316 (2.2)**	**11.4073 (2.1)**	**11.3993 (2.1)**	**11.3957 (2.1)**

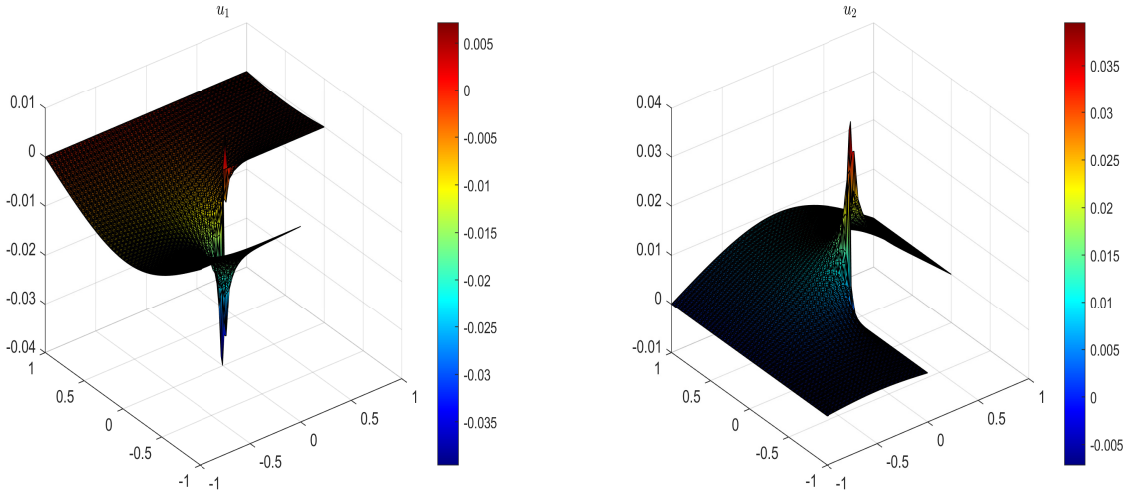

Fig. 4: The components of the fundamental eigenfunction on Ω_2, where $N = 25$.

first value with an increase in the order of interpolations due to the low regularity of the corresponding eigenfunction. Nevertheless, the accuracy is significantly improved for all the approximated values when quadratic interpolations are used instead of the linear ones. The results mentioned here are in analogy with the ones obtained when the AG formulation is used in the simulations, and we prefer not to include them for conciseness of the presentation.

5.4 The cracked square domain

As a final test case, we consider a square domain with a crack defined as $\Omega_3 =]-1,1[^2 \setminus \{(x,y) \in \mathbb{R} : 0 \leq x < 1, y = 0\}$. Sample discretizations of Ω_3 are depicted in Figure 5. In the sequel we report the results of our numerical simulations obtained by, unless it is otherwise stated, using linear interpolations on PS meshes, and taking $\ell = 0.2$, $c_{\boldsymbol{u}} = 0.2$, and $\tau_p = 0.04$, for the stabilized formulations. We report also some results obtained by considering CC

Tab. 15: The first 5 eigenvalues on Ω_2 using the OSGS formulation and P_2 elements on CC meshes.

Ref.	Computed				
	$N = 5$	$N = 10$	$N = 15$	$N = 20$	$N = 25$
1.4756	**1.5446**	**1.5046 (1.3)**	**1.4927 (1.3)**	**1.4873 (1.3)**	**1.4843 (1.3)**
3.5340	**3.5602**	**3.5388 (2.4)**	**3.5357 (2.6)**	**3.5348 (2.6)**	**3.5345 (2.6)**
9.8696	**9.8701**	**9.8696 (4.1)**	**9.8696 (4.0)**	**9.8696 (4.0)**	**9.8696 (4.0)**
9.8696	**9.8701**	**9.8696 (4.1)**	**9.8696 (4.0)**	**9.8696 (4.0)**	**9.8696 (4.0)**
11.3895	**11.4010**	**11.3915 (2.5)**	**11.3902 (2.6)**	**11.3898 (2.6)**	**11.3897 (2.7)**

grids or quadratic interpolations on PS meshes in the sequel. As in the previous case, the reference eigenvalues are taken from [19].

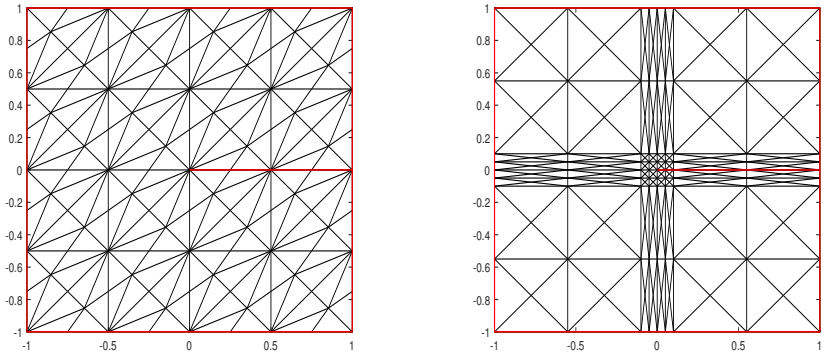

Fig. 5: Sample triangulations of the domain with a crack, Ω_3, with PS mesh where $N = 4$ (left) and internal layer CC mesh when $N = 8$ (right). The boundaries are shown in red.

Additionally to regular solutions, the EVP in this domain also has solutions that are unbounded near the tip of the slit, exhibiting a strong singularity. In particular, the smallest eigenvalue becomes the most crucial one to approximate, as its corresponding eigenfunction belongs to $(H^{1/2-\epsilon}(\Omega))^2$ for any $\epsilon > 0$ (see Figure 6). The same discussion about the treatment of the re-entrant corner as in the L-shape domain case applies to the tip of the crack for this problem, although without a clear identification of a fictitious normal in the present case. For the present instance, we examine the influence of the treatment of enforcing the boundary condition on the approximations by leaving the components of $\boldsymbol{u}$ as free or forcing them to vanish at the tip. We tabulate the corresponding results in Tables 16 and 17 for the former, and Tables 18 and 19 for the latter strategy. Tables 16 and 18 list the results of the SG formulation, whereas Tables 17 and 19 list the ones obtained from the OSGS stabilization. We can easily infer from these tables that the results are more accurate with higher convergence rates when the components of $\boldsymbol{u}_h$ are left to be free in comparison with the case where they are forced to vanish. The difference is very significant in the OSGS formulation, especially in the first eigenvalue, which is approximated with lowest accuracy.

We have observed that all the resulting eigenfunctions related to the values we present are in physically meaningful agreement with the theoretical expectations, with an absence of any spurious mode in a checkerboard pattern. In Figure 6, we plot the components of the fundamental eigenfunction computed using the OSGS formulation when $N = 32$. The components are left free at the tip of the crack (see Table 17) in order to illustrate the singular behavior of the solution vector near it.

To compare the results obtained from different stabilizations for this domain, we list the first 10 eigenvalues obtained from the AG formulation when the components are left free and using the same set of stabilization parameters in Table 20. As before, the OSGS results remain more accurate for each eigenvalue, although a similar convergence tendency is observed in each one.

Tab. 16: The first 10 eigenvalues on Ω_3, SG formulation, u_1, u_2 are free at the tip.

Ref.	Computed				
	$N=2$	$N=4$	$N=8$	$N=16$	$N=32$
1.0341	2.5316	2.4804 (0.1)	2.4723 (0.0)	2.2958 (0.5)	2.0894 (0.8)
2.4674	4.3066	3.3216 (1.1)	2.6162 (4.3)	2.4699 (14.2)	2.4689 (2.3)
4.0469	4.9140	4.0973 (4.1)	4.0654 (2.5)	4.0563 (2.4)	4.0525 (2.3)
9.8696	11.2261	10.1299 (2.4)	9.9673 (2.4)	9.9193 (2.3)	9.8995 (2.3)
9.8696	11.2416	10.1301 (2.4)	9.9674 (2.4)	9.9194 (2.3)	9.8995 (2.3)
10.8449	12.1956	11.1009 (2.4)	10.9444 (2.3)	10.8966 (2.3)	10.8763 (2.2)
12.2649	13.6625	12.5979 (2.1)	12.4445 (1.5)	12.3944 (1.1)	12.3726 (0.8)
12.3370	15.0035	13.3779 (1.4)	12.9190 (1.4)	12.7404 (1.3)	12.6421 (1.3)
19.7392	22.6499	20.3592 (2.2)	20.0052 (2.1)	19.8851 (2.1)	19.8312 (2.1)
21.2441	26.0026	22.9060 (1.5)	22.0858 (1.7)	21.8061 (1.4)	21.6679 (1.3)

Tab. 17: The first 10 eigenvalues on Ω_3, OSGS stabilization, u_1, u_2 free at the tip.

Ref.	Computed				
	$N=2$	$N=4$	$N=8$	$N=16$	$N=32$
1.0341	2.6723	2.5014 (0.2)	2.3973 (0.1)	1.8362 (0.8)	1.4656 (0.9)
2.4674	3.9573	3.0969 (1.2)	2.4736 (6.7)	2.4687 (2.2)	2.4677 (2.1)
4.0469	5.7250	4.2704 (2.9)	4.0846 (2.6)	4.0536 (2.5)	4.0482 (2.4)
9.8696	14.7183	10.4042 (3.2)	9.9669 (2.5)	9.8906 (2.2)	9.8746 (2.1)
9.8696	16.7168	10.4117 (3.7)	9.9674 (2.5)	9.8906 (2.2)	9.8746 (2.1)
10.8449	16.8288	11.5007 (3.2)	10.9714 (2.4)	10.8716 (2.2)	10.8511 (2.1)
12.2649	17.9053	13.0253 (2.9)	12.4791 (1.8)	12.3690 (1.0)	12.3447 (0.4)
12.3370	19.6119	13.6888 (2.4)	12.7776 (1.6)	12.4926 (1.5)	12.3725 (2.1)
19.7392	24.9201	21.0521 (2.0)	20.0963 (1.9)	19.8214 (2.1)	19.7591 (2.0)
21.2441	28.3900	21.4613 (5.0)	21.4403 (0.1)	21.2982 (1.9)	21.2528 (2.6)

Tab. 18: The first 10 eigenvalues on Ω_3, SG formulation, $u_1 = u_2 = 0$ at the tip.

Ref.	Computed				
	$N=2$	$N=4$	$N=8$	$N=16$	$N=32$
1.0341	0.5429	0.7464 (0.8)	0.8771 (0.9)	0.9519 (0.9)	0.9920 (1.0)
2.4674	2.0383	2.3690 (2.1)	2.4438 (2.1)	2.4616 (2.0)	2.4660 (2.0)
4.0469	4.0133	4.0807 (-0.0)	4.0581 (1.6)	4.0500 (1.9)	4.0477 (1.9)
9.8696	10.3409	10.1588 (0.7)	9.9470 (1.9)	9.8892 (2.0)	9.8745 (2.0)
9.8696	10.5393	10.1701 (1.2)	9.9475 (1.9)	9.8892 (2.0)	9.8745 (2.0)
10.8449	10.7668	11.1508 (-2.0)	10.9348 (1.8)	10.8681 (2.0)	10.8507 (2.0)
12.2649	11.0607	11.2899 (0.3)	11.7001 (0.8)	11.9595 (0.9)	12.1060 (0.9)
12.3370	11.3086	12.4285 (3.5)	12.3954 (0.6)	12.3534 (1.8)	12.3412 (2.0)
19.7392	14.0332	20.1339 (3.9)	20.0343 (0.4)	19.8167 (1.9)	19.7588 (2.0)
21.2441	14.6242	20.5661 (3.3)	20.4182 (-0.3)	20.7411 (0.7)	20.9697 (0.9)

So far in this subsection, we have reported the results from interpolations considered on PS type meshes. However, to show the capability of using CC type meshes with increased density along the crack and in the vicinity of the tip with the stabilized formulations, we have tested their approximation features on domains with such strong singularities. A sample triangulation is shown in Figure 5. We list the results that are obtained from P_1 interpolations on these internal layer meshes taking $\ell = 0.25$, $c_{\boldsymbol{u}} = 0.4$, and $\tau_p = 0.125$, using the AG formulation in Table 21 and the

Tab. 19: The first 10 eigenvalues on Ω_3, OSGS stabilization, $u_1 = u_2 = 0$ at the tip.

Ref.	Computed				
	$N = 2$	$N = 4$	$N = 8$	$N = 16$	$N = 32$
1.0341	**5.3986**	**3.7695 (0.7)**	**2.9776 (0.5)**	**2.6047 (0.3)**	**1.9336 (0.8)**
2.4674	**6.2971**	**4.2768 (1.1)**	**3.5556 (0.7)**	**2.6512 (2.6)**	**2.5144 (2.0)**
4.0469	**7.2649**	**4.7126 (2.3)**	**4.0958 (3.8)**	**4.0553 (2.5)**	**4.0484 (2.5)**
9.8696	**16.1213**	**10.4043 (3.5)**	**9.9669 (2.5)**	**9.8906 (2.2)**	**9.8746 (2.1)**
9.8696	**16.7986**	**10.4117 (3.7)**	**9.9674 (2.5)**	**9.8906 (2.2)**	**9.8746 (2.1)**
10.8449	**17.6385**	**11.5576 (3.3)**	**10.9788 (2.4)**	**10.8727 (2.3)**	**10.8512 (2.1)**
12.2649	**19.4200**	**13.4983 (2.5)**	**12.6622 (1.6)**	**12.4241 (1.3)**	**12.3595 (0.8)**
12.3370	**21.2125**	**13.9486 (2.5)**	**12.9150 (1.5)**	**12.5808 (1.2)**	**12.4203 (1.5)**
19.7392	**27.2312**	**21.3475 (2.2)**	**20.0964 (2.2)**	**19.8214 (2.1)**	**19.7591 (2.0)**
21.2441	**30.1025**	**22.1806 (3.2)**	**21.5102 (1.8)**	**21.3059 (2.1)**	**21.2550 (2.5)**

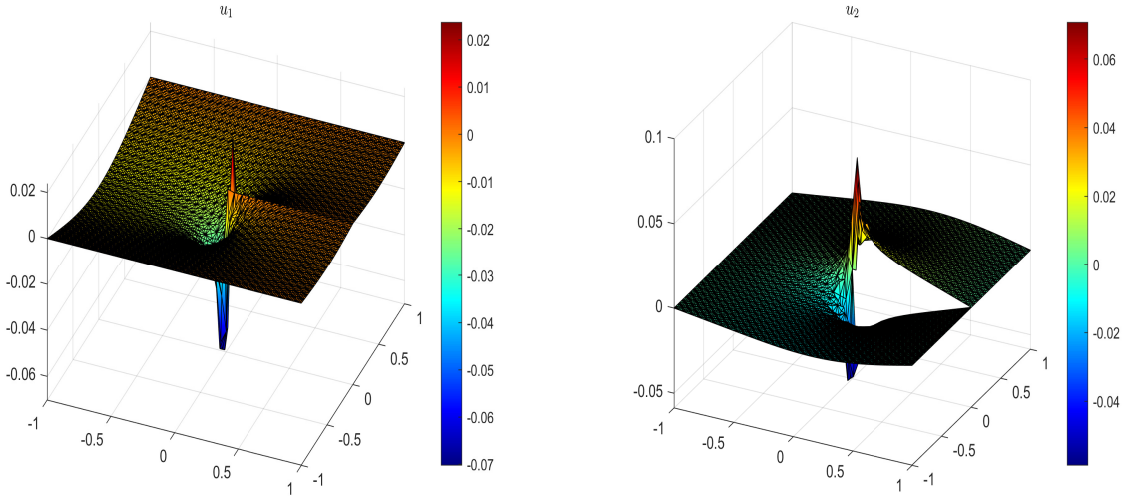

Fig. 6: The components of the fundamental eigenfunction on Ω_3, where $N = 32$.

Tab. 20: The first 10 eigenvalues on Ω_3, AG stabilization, u_1, u_2 free at the tip.

Ref.	Computed				
	$N = 2$	$N = 4$	$N = 8$	$N = 16$	$N = 32$
1.0341	**2.7407**	**2.5124 (0.2)**	**2.4748 (0.0)**	**1.8874 (0.8)**	**1.4198 (1.1)**
2.4674	**4.5001**	**4.0605 (0.4)**	**3.0014 (1.6)**	**2.4688 (8.6)**	**2.4677 (2.2)**
4.0469	**10.7546**	**5.2461 (2.5)**	**4.1090 (4.3)**	**4.0568 (2.7)**	**4.0486 (2.5)**
9.8696	**21.2428**	**10.5965 (4.0)**	**9.9883 (2.6)**	**9.8924 (2.4)**	**9.8747 (2.2)**
9.8696	**22.5337**	**10.5970 (4.1)**	**9.9884 (2.6)**	**9.8924 (2.4)**	**9.8747 (2.2)**
10.8449	**22.9547**	**11.7368 (3.8)**	**11.0081 (2.5)**	**10.8761 (2.4)**	**10.8515 (2.2)**
12.2649	**24.7056**	**13.3075 (3.6)**	**12.5181 (2.0)**	**12.3728 (1.2)**	**12.3448 (0.4)**
12.3370	**36.5179**	**15.3488 (3.0)**	**13.1554 (1.9)**	**12.5279 (2.1)**	**12.3607 (3.0)**
19.7392	**39.0917**	**21.8747 (3.2)**	**20.1941 (2.2)**	**19.8322 (2.3)**	**19.7599 (2.2)**
21.2441	**51.7639**	**25.8291 (2.7)**	**22.3851 (2.0)**	**21.4906 (2.2)**	**21.3091 (1.9)**

OSGS formulation in Table 22. The results in both of these tables put forward the overall acceptable convergence properties, noting as before the relatively lower accuracy in the fundamental eigenvalue that is associated to the singular eigenfunction.

Tab. 21: The first 10 eigenvalues on Ω_3, AG stabilization using CC mesh, u_1, u_2 free at the tip.

Ref.	Computed				
	$N = 8$	$N = 16$	$N = 24$	$N = 32$	$N = 40$
1.0341	**2.5275**	**2.4786 (0.0)**	**2.2677 (0.4)**	**1.8993 (1.2)**	**1.6983 (1.2)**
2.4674	**4.2937**	**3.0951 (1.5)**	**2.4717 (12.3)**	**2.4696 (2.3)**	**2.4688 (2.2)**
4.0469	**5.5933**	**4.0913 (5.1)**	**4.0632 (2.5)**	**4.0552 (2.4)**	**4.0519 (2.3)**
9.8696	**11.1451**	**10.0931 (2.5)**	**9.9549 (2.4)**	**9.9140 (2.3)**	**9.8968 (2.2)**
9.8696	**11.1472**	**10.0931 (2.5)**	**9.9549 (2.4)**	**9.9141 (2.3)**	**9.8968 (2.2)**
10.8449	**12.1662**	**11.0773 (2.5)**	**10.9350 (2.3)**	**10.8924 (2.2)**	**10.8742 (2.2)**
12.2649	**13.6988**	**12.5901 (2.1)**	**12.4388 (1.5)**	**12.3918 (1.1)**	**12.3713 (0.8)**
12.3370	**15.8700**	**13.3026 (1.9)**	**12.7897 (1.9)**	**12.6044 (1.8)**	**12.5135 (1.9)**
19.7392	**22.7109**	**20.3612 (2.3)**	**20.0002 (2.1)**	**19.8825 (2.1)**	**19.8298 (2.1)**
21.2441	**26.1764**	**22.7693 (1.7)**	**21.9533 (1.9)**	**21.6802 (1.7)**	**21.5523 (1.6)**

Tab. 22: The first 10 eigenvalues on Ω_3, OSGS stabilization using CC mesh, u_1, u_2 free at the tip.

Ref.	Computed				
	$N = 8$	$N = 16$	$N = 24$	$N = 32$	$N = 40$
1.0341	**2.5226**	**2.4781 (0.0)**	**2.4108 (0.1)**	**2.1241 (0.8)**	**1.9292 (0.9)**
2.4674	**4.2374**	**2.9578 (1.9)**	**2.4716 (11.7)**	**2.4696 (2.2)**	**2.4688 (2.2)**
4.0469	**4.6380**	**4.0868 (3.9)**	**4.0623 (2.3)**	**4.0549 (2.3)**	**4.0518 (2.2)**
9.8696	**11.0142**	**10.0847 (2.4)**	**9.9536 (2.3)**	**9.9137 (2.2)**	**9.8967 (2.2)**
9.8696	**11.0333**	**10.0849 (2.4)**	**9.9537 (2.3)**	**9.9138 (2.2)**	**9.8967 (2.2)**
10.8449	**11.9657**	**11.0632 (2.4)**	**10.9327 (2.2)**	**10.8918 (2.2)**	**10.8740 (2.1)**
12.2649	**13.4428**	**12.5742 (1.9)**	**12.4362 (1.5)**	**12.3912 (1.1)**	**12.3711 (0.8)**
12.3370	**14.8347**	**13.2343 (1.5)**	**12.8494 (1.4)**	**12.6897 (1.3)**	**12.5957 (1.4)**
19.7392	**22.3994**	**20.3359 (2.2)**	**19.9956 (2.1)**	**19.8813 (2.1)**	**19.8293 (2.0)**
21.2441	**24.0726**	**22.6398 (1.0)**	**22.0059 (1.5)**	**21.7611 (1.3)**	**21.6296 (1.3)**

6 Conclusions

We have studied and numerically validated the characteristics of approximations to the solutions of the Maxwell eigenvalue problem that are obtained using nodal finite elements. Apart from the standard Galerkin formulation used with special (PS type) elements, two stabilized finite element formulations (AG and OSGS) have been implemented successfully to approximate both smooth and singular solutions. The convergence characteristics and error estimates rely on the associated analysis of the source problems. We have shown that the formulations are optimally convergent for a set of algorithmic parameters that are implemented within the stabilized formulations.

The Galerkin formulation, which is singular for the source problem, has been shown numerically to yield reasonable results using PS meshes, as expected. We have also shown that using CC type meshes may lead to spurious solutions even for smooth cases. The OSGS formulation has been shown to work proficiently on the meshes considered

in this study, namely, PS and CC type meshes. The AG formulation has been shown to yield adequate results for smooth solutions, noting the sensitivity to strong singular solutions.

As the main interest of the present study is in the use of nodal elements, a number of strategies of imposition of the boundary condition at the re-entrant corners have been explored. It has been set forth that while leaving the components free may not work well for the standard Galerkin formulation as in the case of the L-shape domain, it functions successfully for both of the stabilized formulations. In addition, it has been shown that a fictitious normal may serve as the best alternative for some problem geometries such as the L-shape domain.

Consequently, we have shown numerically that the stabilized methods can successfully approximate the eigensolutions of Maxwell's system when certain meshes are used, although with some limitations in accuracy in the case of strong singularities. The proposed methods compare very favorably with other formulations due to their ability to acquire the discrete spectrum without the obligation of eliminating the frequencies approximating zero, in addition to their facility of accommodating any order of interpolations and allowing a coupling of different operators.

Acknowledgment: R. Codina acknowledges the support received from the ICREA Acadèmia Research Program of the Catalan Government. D. Boffi is member of INdAM research group GNCS.

References

[1] C. Amrouche, C. Bernardi, M. Dauge, and V. Girault, Vector potentials in three-dimensional non-smooth domains, *Math. Meth. Appl. Sci.*, **21** (1998), 823–864.

[2] I. Babuška and J. Osborn, *Eigenvalue problems*, in Handbook of numerical analysis, Vol. II, Handb. Numer. Anal., II, North-Holland, Amsterdam, 1991, 641–787.

[3] S. Badia and R. Codina, A combined nodal continuous–discontinuous finite element formulation for the Maxwell problem, *Appl. Math. Comput.*, **218** (2011), 4276–4294.

[4] S. Badia and R. Codina, A nodal-based finite element approximation of the Maxwell problem suitable for singular solutions, *SIAM J. Numer. Anal.*, **50** (2012), 398–417.

[5] S. Badia and R. Codina, Stokes, Maxwell and Darcy: a single finite element approximation for three model problems, *Appl. Numer. Math.*, **62** (2012), 246–263.

[6] R. E. Bank and H. Yserentant, On the H^1-stability of the L_2-projection onto finite element spaces, *Numer. Math.*, **126** (2014), 361–381.

[7] G. R. Barrenechea, L. Boulton, and N. Boussaïd, Finite element eigenvalue enclosures for the Maxwell operator, *SIAM J. Sci. Comput.*, **36** (2014), A2887–A2906.

[8] D. Boffi, Finite element approximation of eigenvalue problems, *Acta Numerica*, **19** (2010), 1–120.

[9] D. Boffi, R. Codina and Ö. Türk, Nitsche's prescription of Dirichlet conditions in the finite element approximation of Maxwell's problem. arXiv:2310.18015 [math.NA], 2023.

[10] D. Boffi, S. Gong, J. Guzmán, and M. Neilan, Convergence of Lagrange finite element methods for Maxwell eigenvalue problem in 3D. arXiv:2204.10876 [math.NA], 2022.

[11] D. Boffi, J. Guzmán, and M. Neilan, Convergence of Lagrange finite elements for the Maxwell eigenvalue problem in two dimensions, *IMA J. Numer. Anal.*, (2022).

[12] A. Bonito and J.-L. Guermond, Approximation of the eigenvalue problem for the time harmonic Maxwell system by continuous Lagrange finite elements, *Math. Comput.*, **80** (2011), 1887–1910.

[13] A. Bonito, J.-L. Guermond, and F. Luddens, Regularity of the Maxwell equations in heterogeneous media and Lipschitz domains, *J. Math. Anal. Appl.*, **408** (2013), 498–512.

[14] A. Buffa, P. Ciarlet, and E. Jamelot, Solving electromagnetic eigenvalue problems in polyhedral domains with nodal finite elements, *Numer. Math.*, **113** (2009), 497–518.

[15] S. Caorsi, P. Fernandes, and M. Raffetto, On the convergence of Galerkin finite element approximations of electromagnetic eigenproblems, *SIAM J. Numer. Anal.*, **38** (2000), 580–607.

[16] C. Carstensen, Merging the Bramble-Pasciak-Steinbach and the Crouzeix-Thomée criterion for H^1-stability of the L^2-projection onto finite element spaces, *Math. Comp.*, **71** (2002), 157–163.

[17] S. H. Christiansen, J. Hu, and K. Hu, Nodal finite element de Rham complexes, *Numer. Math.*, **139** (2018), 411–446.

[18] M. Costabel and M. Dauge, Singularities of electromagnetic fields in polyhedral domains, *Arch. Ration. Mech. Anal.*, **151** (2000), 221–276.

[19] M. Dauge, Benchmark computations for Maxwell equations for the approximation of highly singular solutions. https://perso.univ-rennes1.fr/monique.dauge/benchmax.html.

[20] Z. Du and H. Duan, A mixed method for Maxwell eigenproblem, *J. Sci. Comput.*, **82** (2020), 1–37.

[21] H. Duan, Z. Du, W. Liu, and S. Zhang, New mixed elements for Maxwell equations, *SIAM J. Numer. Anal.*, **57** (2019), 320–354.

[22] A. Ern and J.-L. Guermond, Spectral correctness of the continuous finite element stabilized approximation of the first-order form of Maxwell's equations, hal-04478683v2, (2024).

[23] F. Kikuchi, Mixed and penalty formulations for finite element analysis of an eigenvalue problem in electromagnetism, *Comput. Methods Appl. Mech. Eng.*, **64** (1987), 509–521.

[24] P. Monk and L. Demkowicz, Discrete compactness and the approximation of Maxwell's equations in $\mathbb{R}^3$, *Math. Comput.*, **70** (2001), 507–523.

[25] I. Perugia, D. Schötzau, and P. Monk, Stabilized interior penalty methods for the time-harmonic Maxwell equations, *Comput. Methods Appl. Mech. Eng.*, **191** (2002), 4675–4697.

[26] Ö. Türk, D. Boffi, and R. Codina, A stabilized finite element method for the two-field and three-field Stokes eigenvalue problems, *Comput. Methods Appl. Mech. Eng.*, **310** (2016), 886–905.